



# Enhancing the performance of a CO<sub>2</sub> combined refrigeration and power (CRP) cycle driven by engine exhaust gas by using heat exchangers in optimized locations

H.F. Elattar<sup>a</sup>, S.A. Nada<sup>a,b,\*</sup>

<sup>a</sup> Department of Mechanical Engineering, Benha Faculty of Engineering, Benha University, Benha 13511, Qalyubia, Egypt

<sup>b</sup> Egypt-Japan University of Science and Technology, New Borg El-Arab City, 21934 Alexandria, Egypt

## ARTICLE INFO

### Keywords:

Vehicles refrigeration and air conditioning  
Engine waste heat recover  
Combined CO<sub>2</sub> power and refrigeration cycle  
Heat exchanger locations

## ABSTRACT

Carbon Dioxide (CO<sub>2</sub>) has proven its efficiency as a working medium for power and cooling productions in vehicles and refrigerated trucks driven by engine exhaust gases. The main drawbacks of this system are the high/low critical pressure/temperature of the CO<sub>2</sub> which leads to high compressor power and low efficiency. In the present paper two modifications by insertion of two heat exchangers in bottom and top CO<sub>2</sub> compound cycles driven by engine exhaust gas are proposed to overcome on these drawbacks. Energy and exergy analysis are used to evaluate and compare their performances with the basic system. The results show that (i) the feasibility of using the proposed systems was justified and has proven potentials of energy and fuel consumption saving compared to traditional engine + stand-alone refrigerator, (ii) proposed modifications on the basic system (System I) by incorporated heat exchangers (System II and System III) has proven its potential for higher energy efficiency and refrigeration capacity and can recover about 18.33%, 20.38% and 19.22% of the energy of the exhaust gases for driven the compound CO<sub>2</sub> cycle, (iii) parametric, comparison and optimization studies, showed that the proposed system (system II) has the highest refrigeration capacity, energy efficiency and fuel consumption cost saving with optimal values of 20.4%, 0.1819 kg/kWh, 7.1%, respectively.

## 1. Introduction

The transportation sector in the worldwide consumes most of the fossil fuel, especially diesel fuel, compared with other sectors. The diesel fuel annual consumption is in a continues increase with a rate of 1.4% [1]. The diesel fuel consumption increases more and more in refrigerated trucks and air-conditioned transportations and vehicles [1]. Currently there is a worldwide concern regarding the fossil fuel depletion, greenhouse phenomena and the emission problems. The increase of the fuel consumption has severe effect on these problems. To solve these problems the fuel consumption in the transportation sector, especially in air conditioned and refrigerated trucks and vehicles, must be reduced. A lot of studies were conducted in different tracks to reduce this consumptions including using alternatives non-fossil fuels like biofuels [2–4], improving the efficiency of the diesel engines using additive to the diesel fuels likes higher alcohols (butanol, octanol and heptanol)/diesel blends, n-butanol, n-heptanol, and n-octanol to [5–8] in additions to many other effective solutions to increase the engine efficiency and




reduce the fuel consumptions. Among of these effective solutions which are extensively investigated in the recent decades, is the heat recovery in the diesel engines exhaust gases to be utilized in power production and refrigeration effect in the vehicles and the refrigerated trucks. The diesel engine exhaust gas is normally exhausted at high temperature and contains huge amount of thermal energy; about 30–50% of the energy of the fuel consumptions. This high temperature exhaust gas with the quantitatively contained thermal energy give the chances to be recovered by different means including heat to heat exchanging, or power producing to drive many of the auxiliary mechanical or electrical devices in the engine or the vehicle. Also, this energy of the exhaust gas can be recovered to operate the air conditioning and refrigeration systems in vehicles using absorption, adsorption or even vapor compression system.

Various configurations of the combined refrigeration and power (CRP) cycles driven by waste heat recovery from the engine exhaust gases have been proposed and investigated. Recently, CRP cycles have been used in transportation applications including refrigeration and air conditioning of vehicles and chips as well as the refrigerator trucks for

\* Corresponding author at: Department of Mechanical Engineering, Benha Faculty of Engineering, Benha University, Benha 13511, Qalyubia, Egypt.  
E-mail address: [sameh.nada@ejust.edu.eg](mailto:sameh.nada@ejust.edu.eg) (S.A. Nada).

Nomenclature	
$C_{fuel}$	fuel unit cost (\$/kg)
$\dot{E}$	exergy (kW)
$h$	specific enthalpy (kJ/kg)
$\dot{I}$	exergy destruction (kW)
$\dot{m}$	mass flow rate (kg/s)
$P$	Working fluid pressure (MPa)
$\dot{Q}$	heat transfer rate (kW)
$S$	specific entropy (kJ/kg K)
$T$	temperature (°C)
$\dot{W}$	power (kW)
$\dot{W}_{net}$	net output power of CRP system (kW)
<i>Greek symbols</i>	
$\eta$	efficiency
<i>Subscripts</i>	
cg	cold gas
c/comp	compressor
CRP	combined refrigerator and power system (proposed system)
eg	exhaust gas
en	energy
ex	exergy
e/evap	evaporator
f	working fluid (CO <sub>2</sub> )
f,c	working fluid through low pressure compressor
f,e	working fluid through evaporator
f,t	working fluid through turbine
gen	generator
gm	gas mixer
gh	gas heater
hg	hot gas
Hcomp	high pressure compressor
i = 1,2,3,...	index referring to various positions in the system
Lcomp	low pressure compressor
reg	regenerator
ref	refrigeration
SRP	separated refrigerator and power system (traditional system)
SR	Stand-alone refrigerator
t	turbine
t-c	between turbine and compressor
w	water
0	Environmental state
1,2,3, .....	working fluid state points
<i>Abbreviations</i>	
COP	coefficient of performance
CRP	combined refrigeration and power
EXV	Expansion valve
FCCS	fuel consumption cost saving (%)
HEX	internal heat exchanger
Sys-I	modified system-I
Sys-II	modified system-II
Sys-III	modified system-III
SFC	Specific fuel consumption (kg/kWh)

**Table 1**  
Rated condition parameters of target diesel engine & stand-alone refrigerator [40].

Engine	Term	value	
	Engine power	246 kW	
	Engine torque	1242 N m	
	Engine speed	1900 rpm	
	Fuel consumption	48.8 kg/h	
	Mass flow rate of exhaust gas	1372.3 kg/h	
	Temperature of exhaust gas	470.7 °C	
	Exhaust gas composition (mass fraction)	73% N <sub>2</sub> , 6% H <sub>2</sub> O, 15.2% CO <sub>2</sub> , and 5.8% O <sub>2</sub>	
		Refrigeration capacity at refrigeration condition (t <sub>evap</sub> = 0 °C)	10.8 kW
		Fuel consumption at refrigeration condition (t <sub>evap</sub> = 0 °C)	1.45 kg/h
			Refrigeration capacity at freezing condition (t <sub>evap</sub> = -20 °C)
Fuel consumption at freezing condition (t <sub>evap</sub> = -20 °C)			1.70 kg/h

food cooling and reservation. Some of the CRP configurations used a separate system for each of the power and the refrigeration systems operated in a manner where the power cycle is operated by the engine exhaust gas and the refrigeration cycle is operated by the residual heat of the top cycles. Different thermodynamics cycles were utilized in the combined power and refrigeration cycles driven by the exhaust gases like Brayton power cycle combined with ejected refrigerator system [9], ORC combined power cycle with Lithium bromide-absorption refrigeration cycle [10] or with adsorption cycle [11] and Brayton-Rankine power cycle combined with absorption cycle using ammonia-water combination system [12].

Another configuration of the combined power-refrigeration cycle driven by the engine exhaust gases is cascade type where the engine exhaust gases is used to drive the power cycle and the heat rejected from the power cycle is used to drive the refrigeration cycles. Different cycles combinations were proposed for this system including a steam Rankine power cycle with absorption refrigeration cycle using Ammonia water [13–14], Kalina power cycle with ammonia-water absorption cycle [15].

Among these different techniques of the heat recovery from the exhaust gases of diesel engines that gained the interest of different researchers is using combined Organic Rankin cycle for power generation as well as for refrigeration and cooling effect generation. Comprehensive research was conducted in this topic in the current decades due to its high efficiency and effectiveness. The research topics included proposing different configurations of the cycle [16], studying the effect of the organic gas type on the cycle performance and efficiency [17] as well as studying the effect of the operating conditions on the cycle performance and efficiency [18]. Due to the high temperature of the exhaust gases of diesel engines, and its friendly to the environment, the CO<sub>2</sub> combined power and refrigeration cycle showed its suitability and effectiveness in heat recovery from the engine exhaust gas [19–23]. CO<sub>2</sub> has several characteristics to be used as the working fluid of a combined power and refrigeration cycle powered by the heat recovery of the engine exhaust

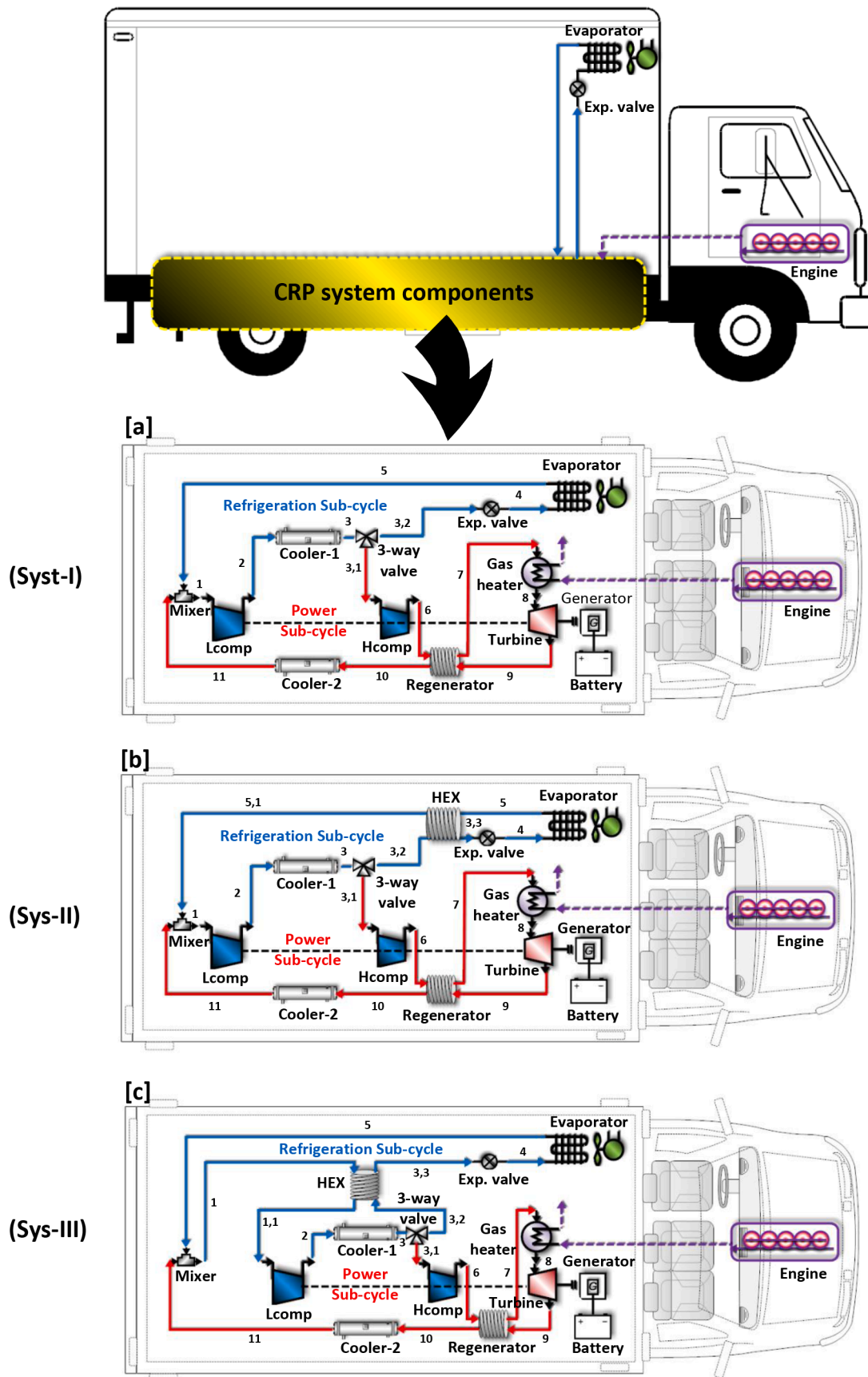


Fig. 1. Schematic diagram of the structure and operation of a refrigerated truck using proposed CRP systems: (a) Sys-I; (b) Sys-II; (c) Sys-III.

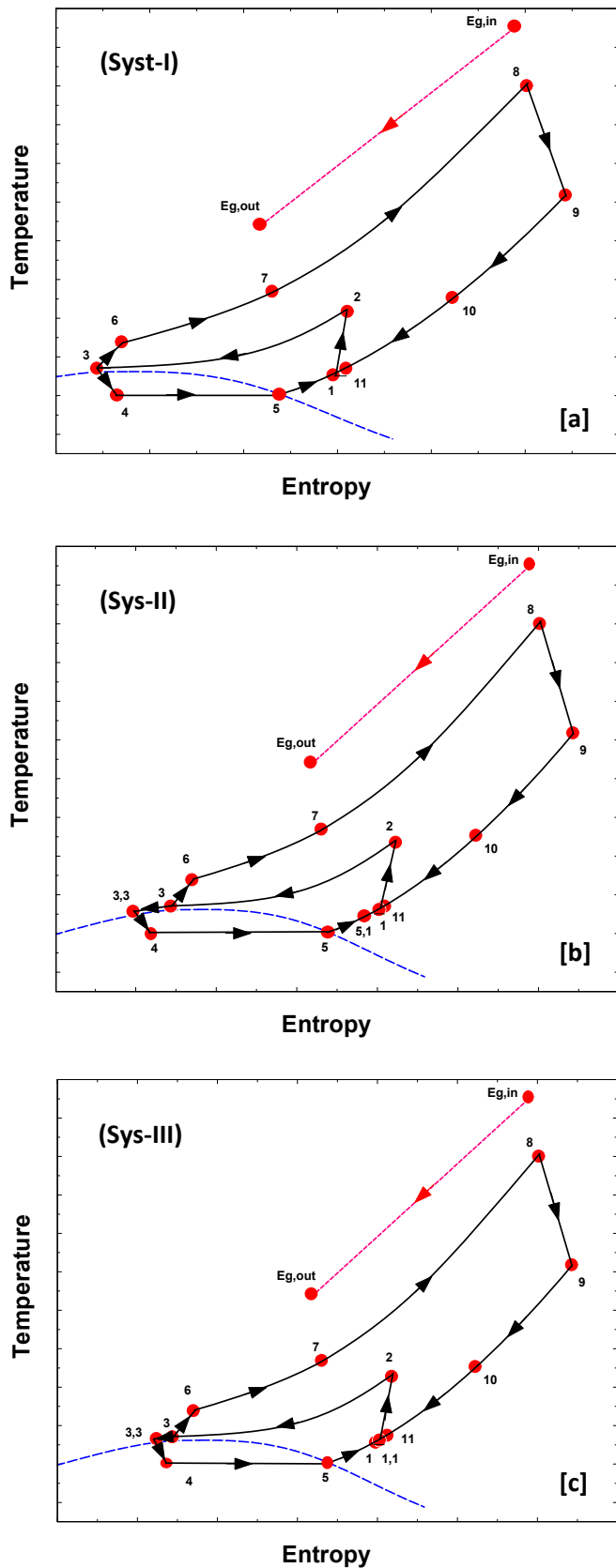


Fig. 2. T-S diagrams of the proposed systems: (a) Syst-I; (b) Syst-II; (c) Syst-III.

gases. Examples of these characteristics are low cost, safe, friendly to the environment, stable at the high temperature of the engine exhaust gases, no limitation of the thermal composition at the temperature level of the exhaust gases, and suitable for the supercritical heat transfer at the temperature range of the exhaust gases [19–23]. Accordingly, CO<sub>2</sub> has proven its effectiveness to be used as the working fluid of many engineering applications including refrigeration and air conditioning systems of vehicles, chips and refrigerator trucks.

For these positive characteristics of CO<sub>2</sub>, a lot of investigations have been conducted for power and cooling generation in heat engine by heat recovery of the exhaust gases using CO<sub>2</sub>-based power cycles. However, a stand-alone CO<sub>2</sub> power cycle driven by engine exhaust gas cannot efficiently utilize the waste heat of the engine exhaust gases. This is due to the high discharge pressure of the turbine which lead to low pressure ratio and enthalpy drop across the turbine as well as a high CO<sub>2</sub> temperature of the turbine discharge. All these drawbacks lead to a low power production and low efficiency of the heat recovered from the engine exhaust gases. Some studies were conducted to overcome on this problem by adding regeneration to recover the discharge heat of CO<sub>2</sub> at the turbine exit, but the studies come out with the conclusion that this heat cannot be totally recovered due to the non-ideal efficiency of the heat exchanger [24]. Other investigation tried to increase by preheating the CO<sub>2</sub> stream at the compressor outlet by recover the heat of the CO<sub>2</sub> at the turbine exit to enhance the cycle efficiency [25]. The enhancement was also limited as the engine exhaust gas still discharged at high temperature and all its thermal energy cannot be recovered [25].

These drawbacks of the high temperature of the CO<sub>2</sub> at the turbine exit can be avoided by utilizing this high temperature source in driving another thermodynamic cycle in a combined system for further recover of the residual heat [26–27]. This combined system is mostly operated on what is known as top and bottom cycles working at high and low temperature levels, respectively. The top cycle can be efficiently used for power generation and the bottom cycle can be also efficiently used for the refrigeration effect. So, it is very logically and feasible to use this combined cycle driven by the heat recovered from the exhaust gases to produce the electrical/mechanical powers as an auxiliary power needed for auxiliary mechanical/electrical devices and the vehicles/trucks batteries from the top cycle as well as the production of the refrigeration demand in the bottom cycle needed for a refrigerated truck or air conditioning space in the vehicle.

An efficient configuration of the combined power and refrigeration cycle driven by the waste heat recovery of the engine exhaust gases is the use of CO<sub>2</sub> to drive both the power and the refrigeration cycle. CO<sub>2</sub> has proven its suitability as a working fluid for a power cycle and a refrigeration/air conditioning cycles [28]. The integration between the power and the refrigeration cycles is achieved by coupling the compression process for power and refrigeration cycles [29,30].

Several investigations were conducted to study and enhance the performance of the CO<sub>2</sub> based power and refrigeration cycles driven by the heat recovered from the engine exhaust gases. Gutierrez et al [31] presented energy, exergy, and economic comparative study of two different Brayton S- CO<sub>2</sub>-ORC configurations for different organic working fluids. They reported the increase of the system thermal efficiency and the decrease of the specific fuel consumption in case of using Brayton S- CO<sub>2</sub> system. Sun et al. [32] proposed a composition tunable combined refrigeration and power cycles driven by heat recovery from the vehicle exhaust gases based on liquid separation condenser to two different streams of different concentrations, one for the top cycle for power production with high CO<sub>2</sub> concentration and the other is for the bottom refrigeration cycle with low CO<sub>2</sub> concentration. Sahu et al. [33] Presented a parametric study for both the simple transcritical CO<sub>2</sub> refrigeration cycle and the combined refrigeration-power cycle. It was reported that the COP and second-law efficiency of the combined refrigeration power cycle is significantly higher than those of the simple refrigeration cycle. Wang et al. [34] proposed a new thermodynamic arrangement to enhance the design of recuperative in the power and

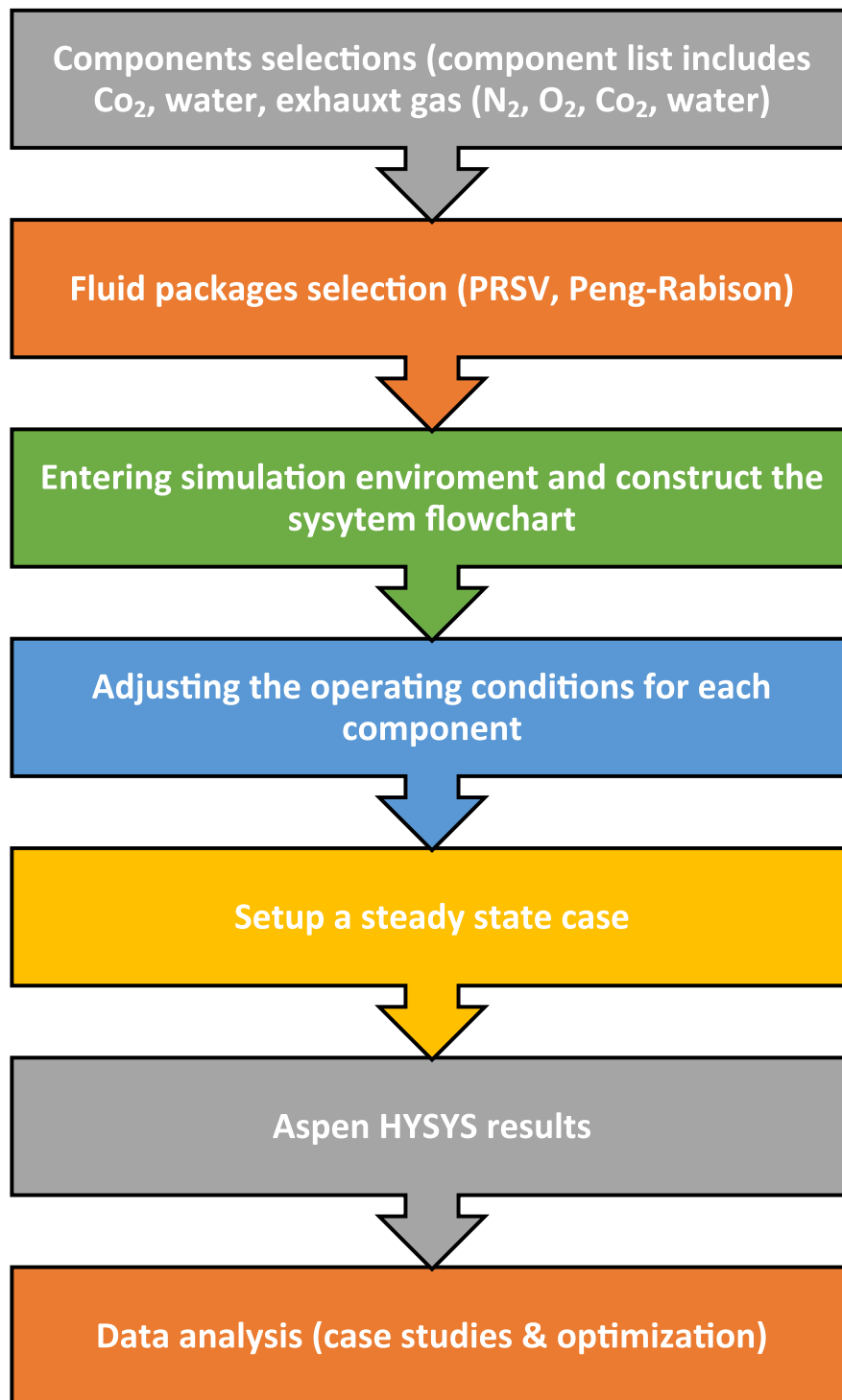


**Fig. 3.** Simulation steps flow diagram in Aspen HYSYS.

refrigeration CO<sub>2</sub> based combined systems for marine engines of high-temperature waste exhaust gases. Nader et al. [35] investigated the fuel consumption savings of a series of hybrid electric vehicle using Brayton cycle for engine exhaust heat recovery using exergy analysis. Song et al. [36]. Investigated the replacement of the conventional hydrofluorocarbon (HFC) and R407C refrigerant used in vehicle air conditioning system by CO<sub>2</sub> refrigerant. The results showed that the performance of the CO<sub>2</sub> system in heating is better, but it is no so good for cooling. Song et al. [37] studied the performance of the transcritical CO<sub>2</sub> air conditioning system used in the electric buses under different

operating and outdoor conditions using energy-exergy analysis system and it was reported that the performance is dramatically decreases with the increase of the outdoor temperature. Fartaj et al. [38] identified, based on the second law analysis, the main factors that influence the performance of the refrigeration systems that use transcritical CO<sub>2</sub> refrigerant. The study reported that the compressor process and the gas cooling have the largest exergy within the system. Sharma et al. [39] studied the effect of the different operating conditions and parameters on the performance of a waste heat recovery system used in ship boards in the supercritical CO<sub>2</sub> Brayton cycle for power and cooling production.

**Table 2**  
Operating parameters conditions.

Parameter	Value / Range
Turbine inlet pressure, $P_8$	10–30 MPa
Turbine inlet temperature, $T_8$	200–450 °C
Intermediate pressure, $P_2$	8–30 MPa
Water cooler inlet temperature, $T_{w,in}$	20–40 °C
Evaporating temperature, $T_4$	–20 to 0 °C
Water flow rate of cooler – 1, $\dot{m}_{w1}$	1.5 kg/s
Water flow rate of cooler – 2, $\dot{m}_{w2}$	0.5 kg/s
Efficiency of electrical generator, $\eta_{gen}$ , [53]	90%
Efficiency of turbine-compressors connection, $\eta_{t-c}$ , [53]	90%

The results show that the top and bottom cycles integration for power and cooling enhanced the system overall efficiency by 10% with increasing the net power by 25%. Zhang et al. [40] proposed a new supercritical CO<sub>2</sub> power cycle to recover the heat of the exhaust gases. Energy-exergy analysis is presented to study the effect of the different operating parameters and conditions on the system performance. They concluded that the proposed system could recover the heat in the exhaust gases with an efficiency of 74.83%.

Ouyang et al. [41] developed a dynamic model of engines exhaust waste heat recovery system to drive the refrigeration system of the vehicle based on CO<sub>2</sub> performance optimization and the adjustment of the operating condition for higher output power. Shi et al. [42] proposed three operating modes for the CO<sub>2</sub> cycle used for refrigeration and power production in a refrigerated trucks operated by the waste heat recovery of the exhaust gases. The three suggested modes are for different demands of the refrigeration and power loads at different operating conditions. The modes were for full refrigeration load, combined refrigeration and power loads, and full power load. They reported that the proposed system showed considerable potential for energy saving and it can provide greater refrigeration and power loads full refrigeration and full power modes.

Different configurations of the Brayton waste heat recovery were proposed and compared with the simple Brayton cycle. Musharavati et al. [43] examined the effects of adding thermoelectric generation unit (TEG) in a recompression Brayton ad it was reported that adding the TEG to the system can increase the net output power and enhance the second law efficiency of the combined system. Sanchez et al. [44] experimentally studied the enhancement of the performance and the COP of the CO<sub>2</sub> refrigeration plants by using internal heat exchangers in the cycle. They concluded that a general enhancement of the performance and the COP due to the use of the heat exchangers in the cycles whatever the location of the heat exchanger. A maximum enhancement of 13% in the performance (COP) was obtained when two heat exchangers are used in the cycle. Wang et al. [45]. Introduced a new polygeneration system including a gas turbine cycle, a supercritical CO<sub>2</sub>-Brayton cycle, Organic Rankine cycle (ORC), and absorption refrigeration cycle. The heat in the exhaust gases of the gas turbine was used to drive the CO<sub>2</sub>, Organic Rankin cycle and the bottom absorption cycle. Li et al. [46] experimentally tested the performance of the secondary loop refrigeration system based on energy-exergy concept for different refrigerants for the selection of the best global warming refrigerant. Xin et al. [47] presented a new combined supercritical CO<sub>2</sub> cycle configuration based on analytical investigation and they reported that the proposed cycle can achieve the cycle efficiency of 53.58%. Banik et al. [48] introduced parametric study and optimization of a transcritical CO<sub>2</sub> power cycle with a modification of recompresses part of the refrigerant before entering precooler for higher cycle efficiency. They reported that the proposed system can work for heat recovery from exhaust gases at low temperature of 200 C.

Mohanaraj and Abraham [49] reviewed and compared in a review paper the performance of the different refrigerants used in the vehicle air conditioning system. They reported that the CO<sub>2</sub> refrigerant will recently dominate other refrigerants in the vehicle air conditioning

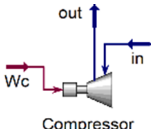
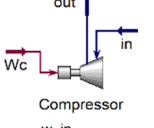
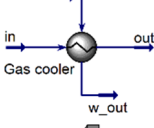
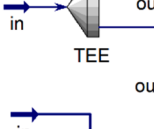
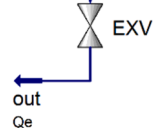
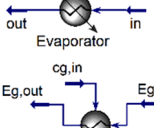
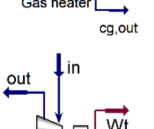
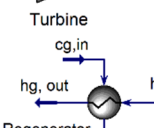
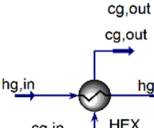
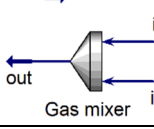
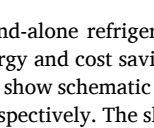
system, especially in the electric vehicles in a low temperature weather condition, due to its good thermodynamic, thermophysical and environmental properties. They recommended the use of secondary bottom loop configurations to avoid the risk of the flammable to occur. Vashist and Rakshit [50] reviewed and compared the different air conditioning systems used in automobile for a sustainable solution and reducing the specific fuel consumption of the engine and it was recommended to move the environmentally friendly refrigerant system like CO<sub>2</sub>. Rony et al. [51] presented a review paper on the most recent developments of transcritical CO<sub>2</sub> system used in the heat pump including auxiliary internal component to enhance the performance as well as the different applications including the air conditioning of the vehicles. Dilshad et al. [52] presented a cortical review of using CO<sub>2</sub> refrigerant in heating and cooling system all over the world. The review highlighted the advantages, barriers and challenges and barriers of the commercial use of CO<sub>2</sub> in refrigeration and heating system all over the world. Barta et al. [53] presented a literature review of using CO<sub>2</sub> as a refrigerant in refrigeration and air conditioning systems. The advantages and disadvantages of the CO<sub>2</sub> refrigerant are highlighted in this review. Also, all the cycle modifications proposed in the literature to overcome on the disadvantages are discussed in this critical review.

The literature review proved that since discovering Carbon Dioxide (CO<sub>2</sub>) as a refrigerant three decades ago and due to its negligible global warming potential, stability, and its non-toxicity, non-flammability, and low cost allows its use in many vapor compression cycle applications. The main disadvantages of the CO<sub>2</sub> are its high critical pressure and low critical temperature which leads to high compressor power especially under high-ambient conditions. This disadvantage encouraged a lot of researchers to work and look for cycle modifications to reach high coefficient of performance (COP). One of these modifications which was agreed by many researchers was using compound cycles for power and cooling productions. However even with this solution the literature showed that there are a lot of other modifications which can be used with this solution to improve the COP of the system. The gap in this area is still open and need to much more work and modification to reach to a configuration of optimum performance. The aim of the current paper is to look for optimum cycle with the insertion of internal heat exchangers in CO<sub>2</sub> power and refrigeration compound cycle drive by the engine exhaust gas at different locations searching for the configuration of optimum performance. To achieve this purpose, a simulation model with a power software is needed for simulating the operation of the proposed CRP systems. To justify the goal of this research, it is interested to look at how much energy is saved in the proposed combined refrigeration and power CO<sub>2</sub> cycles driven by the engine exhaust gases of a refrigerated truck compared to a traditional system that runs the engine and the stand-alone refrigerator. The other part of the study's novelty is the use of Aspen HYSYS Software (AspenTech, Bedford, MA, USA) [54] as a commercial process simulator for the modeling, solution and analysis of the results of proposed systems, which benefits from specialized fluid packages, credibility, and robustness.

## 2. Systems descriptions

To perform the present work, the performance of a refrigerated truck with a 246-kW engine [42] is investigated under its basic condition and the proposed modifications in the cycle. The composition of the exhaust gas was tabulated in Table 1 under the assumption of perfect combustion of diesel fuel. This composition is used to determine the heat source's thermodynamic properties. The suggested CRP systems' heat source condition is chosen as the rated condition of the engine, whose parameters are presented in Table 1. Prior to delivering the CRP systems, a stand-alone Carrier Supra 950 with a small-scale individual diesel engine is employed to supply the refrigerated capacity. This is considered and named as the engine and the stand-alone refrigerator. Table 1 also shows the refrigeration capacity and associated fuel consumption of the stand-alone refrigerator. The proposed CRP systems are expected to

**Table 3**  
Energy and exergy equations and modelling assumptions of the proposed systems components.

Component	Symbol	Characteristic equations [53]	Modelling assumptions
Lcomp		$\dot{W}_{Lcomp} = \dot{m}_{f,c}(h_2 - h_1)$ $= \dot{m}_{f,c}(h_{2,s} - h_1)/\eta_c \dots (\text{Sys} - \text{I} \& \text{Sys} - \text{II})$ $= \dot{m}_{f,c}(h_{2,s} - h_{1,1})/\eta_c \dots (\text{Sys} - \text{III})$ $\dot{I}_{Lcomp} = \dot{E}_1 - \dot{E}_2 + \dot{W}_{Lcomp} \dots (\text{Sys} - \text{III})$	$\eta_c = 80\%$ , [53] Polytropic method: Shultz Operation mode: centrifugal
Hcomp		$\dot{W}_{Hcomp} = \dot{m}_{f,t}(h_6 - h_{3,1}) = \dot{m}_{f,t}(h_{6,s} - h_{3,1})/\eta_c$ $\dot{I}_{Hcomp} = \dot{E}_{3,1} - \dot{E}_6 + \dot{W}_{Hcomp}$	$\eta_c = 80\%$ , [53] Polytropic method: Shultz Operation mode: centrifugal
Cooler		$\dot{Q}_{cooler-1} = \dot{m}_{f,c}(h_2 - h_3) = \dot{m}_{w1}(h_{w1,out} - h_{w1,in})$ $\dot{Q}_{cooler-2} = \dot{m}_{f,t}(h_{10} - h_{11}) = \dot{m}_{w2}(h_{w2,out} - h_{w2,in})$ $\dot{I}_{cooler-1} = \dot{E}_2 - \dot{E}_3 + \dot{E}_{w1,in} - \dot{E}_{w1,out}$ $\dot{I}_{cooler-2} = \dot{E}_{10} - \dot{E}_{11} + \dot{E}_{w2,in} - \dot{E}_{w2,out}$	Minimum approach: 5 °C Heat exchanger model: Simple end point $\Delta P$ shell-side = 0 kPa $\Delta P$ tube-side = 0 kPa
Three-way valve		$\dot{m}_{f,c}h_3 = \dot{m}_{f,t}h_{3,2} + \dot{m}_{f,t}h_{3,1}$ $\dot{I}_{3-way valve} = \dot{E}_3 - \dot{E}_{3,1} - \dot{E}_{3,2}$	The same temperatures: $t_3 = t_{3,1} = t_{3,2}$
Expansion valve		$\dot{m}_{f,c}h_{3,2} = \dot{m}_{f,c}h_4 \dots (\text{Sys} - \text{I})$ $\dot{m}_{f,t}h_{3,3} = \dot{m}_{f,t}h_4 \dots (\text{Sys} - \text{II} \& \text{Sys} - \text{III})$ $\dot{I}_{EXV} = \dot{E}_{3,2} - \dot{E}_4 \dots (\text{Sys} - \text{I})$ $\dot{I}_{EXV} = \dot{E}_{3,3} - \dot{E}_4 \dots (\text{Sys} - \text{II} \& \text{Sys} - \text{III})$	
Evaporator		$\dot{Q}_{evap} = \dot{m}_{f,e}(h_5 - h_4)$ $\dot{I}_{evap} = \dot{E}_4 - \dot{E}_5 - \dot{E}_{evap}$	Minimum approach: 5 °C $x_5 = 1$ $\Delta P = 0$ kPa
Gas heater		$\dot{Q}_{gh} = \dot{m}_{f,t}(h_8 - h_7) = \dot{m}_{Eg}(h_{Eg,in} - h_{Eg,in})$ $\dot{I}_{gh} = \dot{E}_7 - \dot{E}_8 + \dot{E}_{cg,in} - \dot{E}_{cg,out}$	Minimum approach: 30 °C Heat exchanger model: Simple end point $\Delta P$ shell-side = 0 kPa $\Delta P$ tube-side = 0 kPa
Turbine		$\dot{W}_t = \dot{m}_{f,t}(h_8 - h_9) = \dot{m}_{f,t}(h_8 - h_{9s})\eta_t$ $\dot{I}_t = \dot{E}_8 - \dot{E}_9 - \dot{W}_t$	$\eta_t = 70\%$ , [53]
Regenerator		$\dot{Q}_{reg} = \dot{m}_{f,t}(h_7 - h_6) = \dot{m}_{f,t}(h_9 - h_{10})$ $\dot{I}_{reg} = \dot{E}_6 - \dot{E}_7 + \dot{E}_9 - \dot{E}_{10}$	Minimum approach: 30 °C Heat exchanger model: Simple end point $\Delta P$ shell-side = 0 kPa $\Delta P$ tube-side = 0 kPa
HEX		$\dot{Q}_{HEX} = \dot{m}_{f,e}(h_{3,2} - h_{3,3}) = \dot{m}_{f,e}(h_{5,1} - h_5) \dots (\text{Sys} - \text{II})$ $\dot{Q}_{HEX} = \dot{m}_{f,e}(h_{3,2} - h_{3,3}) = \dot{m}_{f,c}(h_{1,1} - h_1) \dots (\text{Sys} - \text{III})$ $\dot{I}_{HEX} = \dot{E}_{3,2} - \dot{E}_{3,3} + \dot{E}_5 - \dot{E}_{5,1} \dots (\text{Sys} - \text{II})$ $\dot{I}_{HEX} = \dot{E}_{3,2} - \dot{E}_{3,3} + \dot{E}_1 - \dot{E}_{1,1} \dots (\text{Sys} - \text{III})$	Minimum approach: 10 °C Heat exchanger model: Simple end point $\Delta P$ shell-side = 0 kPa $\Delta P$ tube-side = 0 kPa
Gas mixer		$\dot{m}_{f,c}h_1 = \dot{m}_{f,e}h_5 + \dot{m}_{f,t}h_{11} \dots (\text{Sys} - \text{I} \& \text{Sys} - \text{III})$ $\dot{m}_{f,t}h_1 = \dot{m}_{f,e}h_{5,1} + \dot{m}_{f,t}h_{11} \dots (\text{Sys} - \text{II})$ $\dot{I}_{gm} = \dot{E}_5 + \dot{E}_{11} - \dot{E}_1 \dots (\text{Sys} - \text{I} \& \text{Sys} - \text{III})$ $\dot{I}_{gm} = \dot{E}_{5,1} + \dot{E}_{11} - \dot{E}_1 \dots (\text{Sys} - \text{II})$	Automatic pressure assignment: Equalize all

replace this stand-alone refrigerators and produce other extra power, resulting in energy and cost savings on the long run.

Figs. 1 and 2 show schematic diagrams and T-s diagrams of proposed CRP systems, respectively. The shared Low compressor and cooler-1 are used to connect the power and refrigeration sub-cycles, and a three-way valve is used to achieve split-flow. Three CRP systems are proposed in this study (i.e., Sys-I, Sys-II, and Sys-III). The systems are made up of a supercritical CO<sub>2</sub> power cycle (S-CO<sub>2</sub>) and a transcritical CO<sub>2</sub>

refrigeration cycle (T-CO<sub>2</sub>) with two separate coolers and different suggested internal heat exchanger at the bottom and top cycles (Sys-II, and Sys-III). In these systems, the power cycle absorbs heat from the exhaust gas, and the power generated in the turbine, is used to drive the compressors in both the power sub-cycle and the refrigeration sub-cycle. Because the temperature of the CO<sub>2</sub> stream exiting the turbine remains high, a regenerator is used to further utilize the energy and improve the thermal efficiency of the power cycle. Because this system will be used

**Table 4**  
Validation of the present model with available reference results [54].

State parameters						Performance parameters					
Ref. [54], Experimental data						$\dot{W}_{comp}$ (W)			COP		
$\dot{Q}_{evap}$ (W)	$T_{evap}$ (°C)	$T_{comp,in}$ (°C)	$P_{comp,out}$ (bar)	$T_{cooler,out}$ (°C)	$\eta_{comp,overall}$ (%)	Ref. [52], Exp.	Present model	Error (%)	Ref. [52], Exp.	Present model	Error (%)
351.65	-11.30	35.38	89.71	35.24	46.30	326.47	348.02	6.19	1.08	1.01	6.35
525.11	-2.03	35.62	90.37	35.23	54.80	343.65	373.94	8.10	1.56	1.40	9.81
832.70	9.48	35.42	90.14	36.45	65.70	335.11	373.97	10.39	2.49	2.23	10.40
469.09	-11.58	31.06	84.95	31.94	56.00	331.57	353.45	6.19	1.42	1.33	6.20
649.51	-1.77	31.56	84.98	31.94	60.60	351.66	368.66	4.61	1.85	1.76	4.61
842.02	5.32	31.83	85.78	32.11	64.50	360.06	381.33	5.58	2.29	2.21	3.37
Ref. [54], Numerical data						$\dot{W}_{comp}$ (W)			COP		
$\dot{Q}_{evap}$ (W)	$T_{evap}$ (°C)	$T_{comp,in}$ (°C)	$P_{comp,out}$ (bar)	$T_{cooler,out}$ (°C)	$\eta_{comp,overall}$ (%)	Ref. [52], Num.	Present model	Error (%)	Ref. [52], Num.	Present model	Error (%)
367.25	-9.56	34.39	89.71	35.24	46.8	323.12	349.64	7.58	1.14	1.05	7.54
544.63	-1.62	34.52	90.37	35.23	52.6	357.79	381.84	6.30	1.52	1.43	6.29
816.03	9.53	34.44	90.14	36.45	62.8	350.87	363.26	3.41	2.33	2.25	3.38
488.58	-10.27	31.19	84.95	31.94	55.3	335.54	358.00	6.27	1.46	1.36	6.27
695.93	-0.99	31.17	84.98	31.94	61.7	345.22	386.52	10.69	2.02	1.80	10.65
851.32	5.09	31.03	85.78	32.11	65.6	345.59	385.73	10.41	2.46	2.21	10.43

on a refrigerated truck, both coolers are water-cooled and integrated with a common air-cooled type heat exchanger. A refrigeration system of this type aims to provide sufficient cooling for the refrigerated truck cabinet to preserve food or other goods for refrigerating and freezing while transporting. Fig. 2 depicts the temperature-specific entropy (T-S) diagrams of the proposed CRP systems. The proposed system's processes, structure, and operation are depicted in Fig. 3 and described below.

In Sys-I (see Fig. 1-a and Fig. 2-a), a portion of the supercritical CO<sub>2</sub> from the three-way valve flows into the high-pressure compressor (Hcomp) and reaches a high-pressure state (state 6), after which it is heated by the CO<sub>2</sub> discharging steam in the regenerator (state 7) and exhaust gas in a gas heater (state 8). The high-pressure and high-temperature CO<sub>2</sub> flows into the turbine and generates work (state 9), after which the CO<sub>2</sub> gas outlet from the turbine is cooled in the regenerator (state 10) and then in a low-pressure cooler, cooler-2 (state 11). The remaining supercritical CO<sub>2</sub> from the three-way valve passes through an expansion valve and exits as two-phase flow (state 4). In an evaporator, liquid CO<sub>2</sub> evaporates and provides refrigeration capacity while leaving the evaporator saturated vapour (state 5). The cold and hot gases are mixed in a mixer (states 5 and 11), and the resulting mixture enters the low-pressure compressor (state 1) before being cooled by a cooler-1 (state 3). The operation and components of the Sys-I are like those described by Yao et al. [55] and it taken as a reference and basic system for the other two improved and modified systems (Sys-II, and Sys-III).

In Sys-II (see Fig. 1-b and Fig. 2-b), the system operation and components are modified from Sys-I by adding HEX between the part of supercritical CO<sub>2</sub> that comes from the three-way valve before entering the expansion valve (state 3,2) and the saturated vapour that exits the evaporator (state 5) to improve the refrigeration sub-cycle COP and thus the overall system efficiency. In Sys-III (see Fig. 1-c and Fig. 2-c), (see Fig. 1-a and Fig. 2-a), the HEX is added between the supercritical CO<sub>2</sub> stream that comes from the three-way valve before entering the expansion valve (state 3,2) and the mixing stream that exits from the gas mixer (state point 1) in order to achieve the most efficient system operation when compared to Sys-I.

### 3. Modeling and assumptions

To investigate the thermodynamic performance of the proposed CRP systems, a simulation model based on Aspen HYSYS® Software

(AspenTech, Bedford, MA, USA) [54] is used. Scholars and engineers have recognized Aspen HYSYS for its dependability and ability to assess the performance of complex industrial processes. Because the Aspen HYSYS platform is user-friendly to a large extent, it allows for the optimization of conceptual design and operations. For steady-state modeling, Aspen HYSYS has a solid approach. Fig. 3 depicts the fundamental steps of the preset study's steady-state simulation. Aspen HYSYS is a powerful process simulator that includes a large library of pre-built component models and property packages. It enables the static/dynamic modeling of a wide range of complex chemical/hydrocarbon fluid-based processes by simply connecting different modules using material and energy streams. Hence, a simulation model in Aspen HYSYS for CRP systems allows easy integration with various energy systems such as compressors, turbines, gas coolers, gas heaters, heat exchangers, evaporators, expansion valves, etc.

For modeling, the following assumptions are used:

- The ambient temperature of 25 °C remains constant and it is used as the reference temperature.
- The entire system operates in a steady state.
- In all pipes and components, heat and pressure loss are ignored.
- The evaporator's outflows are saturated vapour.
- The throttling valve process is isenthalpic.
- To avoid corrosion of the pipe and heat exchanger, the exhaust gas temperature is higher than the acid dew point (120 °C) after heat transfer.
- The pressure levels in the cooler-2 and evaporator are the same.
- The isentropic and mechanical efficiencies of the compressors and turbines are maintained constant,
- Cooler-1 and cooler-2 pinch points are located between the fluid and ambient temperatures. Tables 2 and 3 show a variety of operating parameter and modeling assumption values.

#### 3.1. Energy analysis

The mass and energy equations are obtained to simulate the thermodynamic processes in CRP based on the above assumptions and the first law of thermodynamics. The calculated preset flow of working fluid in the evaporator and gas heater ( $\dot{m}_e^*$  and  $\dot{m}_g^*$ ) is based on the refrigeration capacity and waste heat conditions that shown in Table 1.

In the 3-way valve and gas mixer, the mass conservation equation is



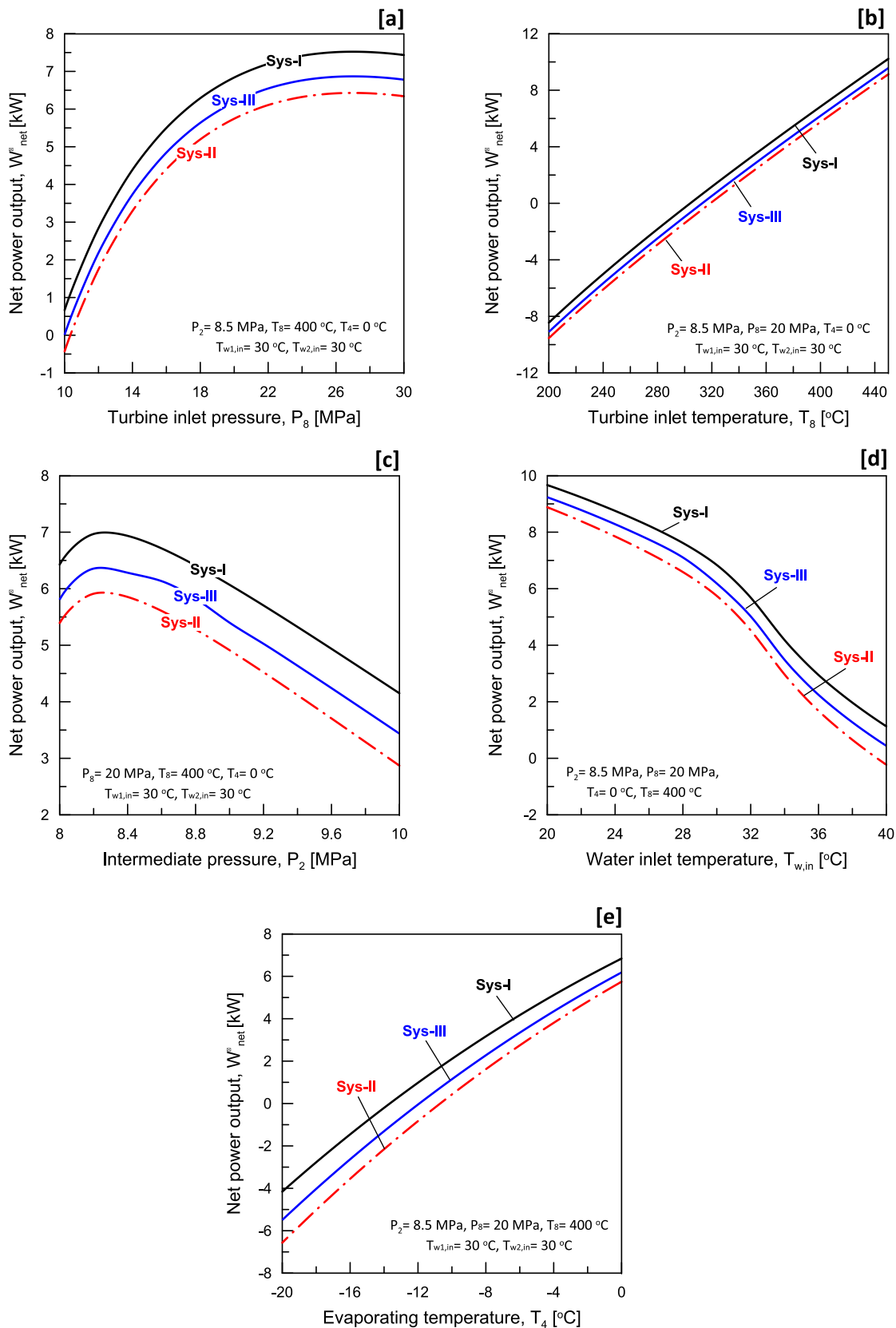


Fig. 4. Variations of net power output,  $\dot{W}_{net}$  with various: (a) Turbine inlet pressure; (b) Turbine inlet temperature; (c) Intermediate pressure; (d) Water inlet temperature; (e) Evaporating temperature.

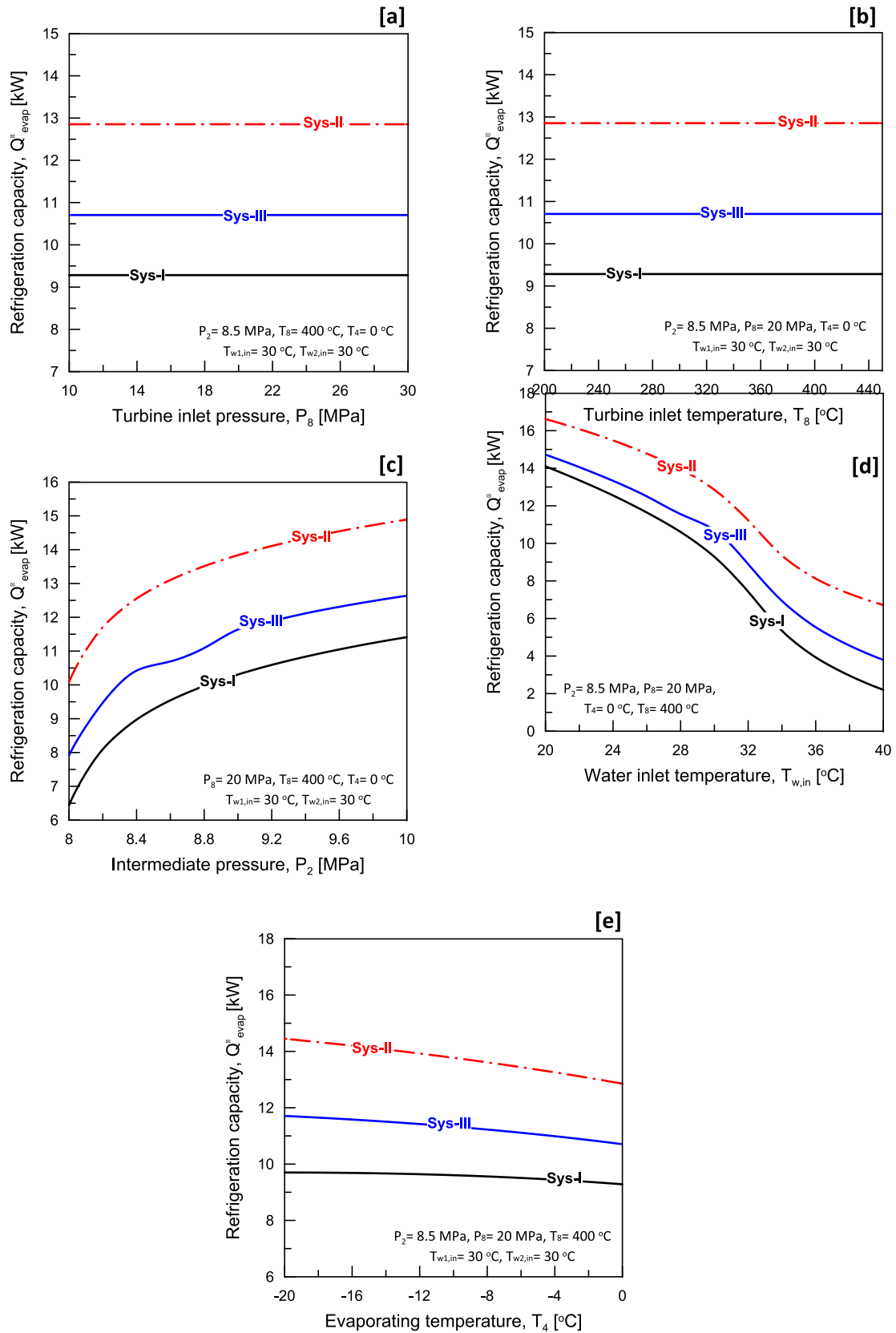


Fig. 5. Variations of refrigeration capacity,  $\dot{Q}_{evap}$  with various: (a) Turbine inlet pressure; (b) Turbine inlet temperature; (c) Intermediate pressure; (d) Water inlet temperature; (e) Evaporating temperature.

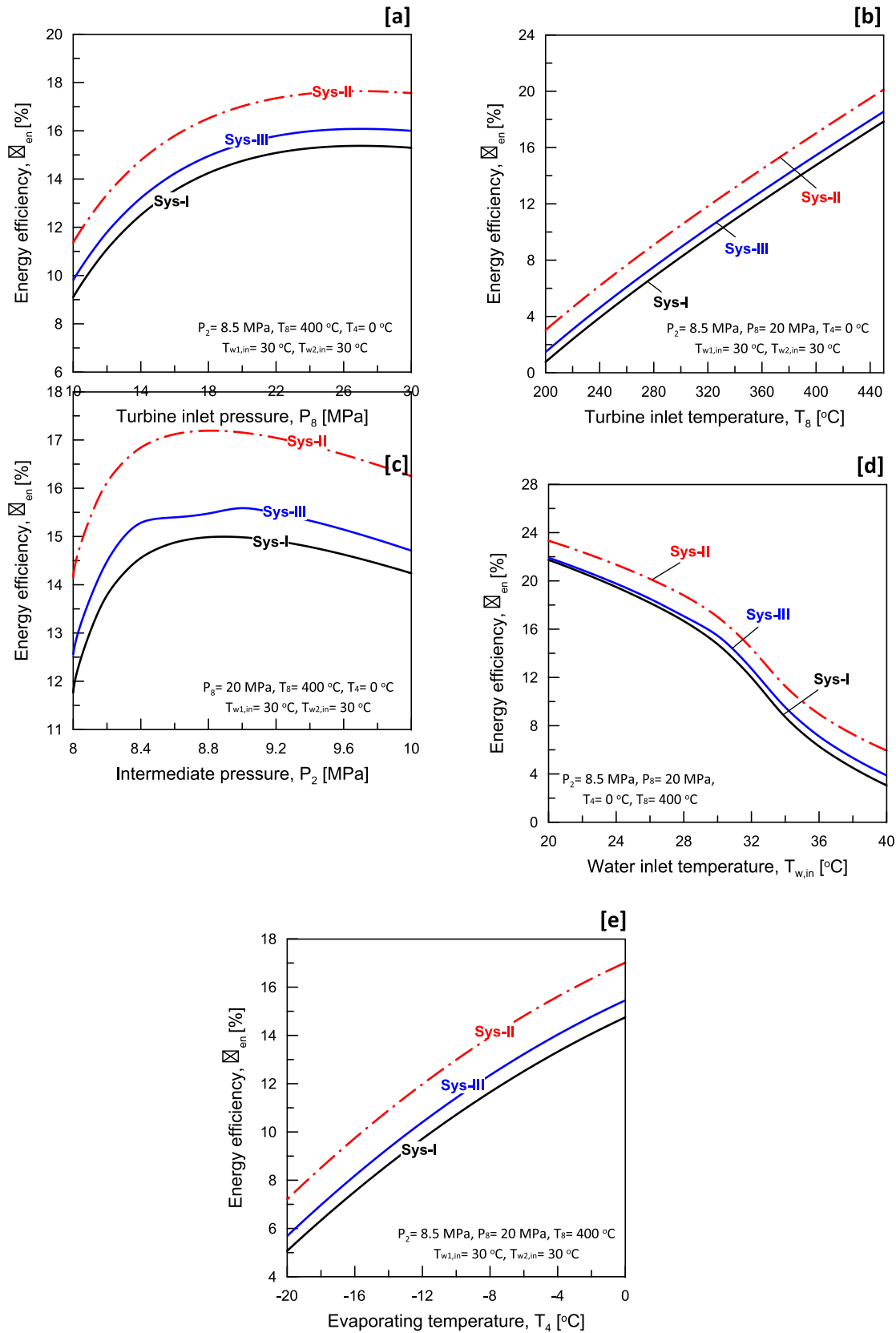


Fig. 6. Variations of energy efficiency,  $\eta_{en}$  with various: (a) Turbine inlet pressure; (b) Turbine inlet temperature; (c) Intermediate pressure; (d) Water inlet temperature; (e) Evaporating temperature.

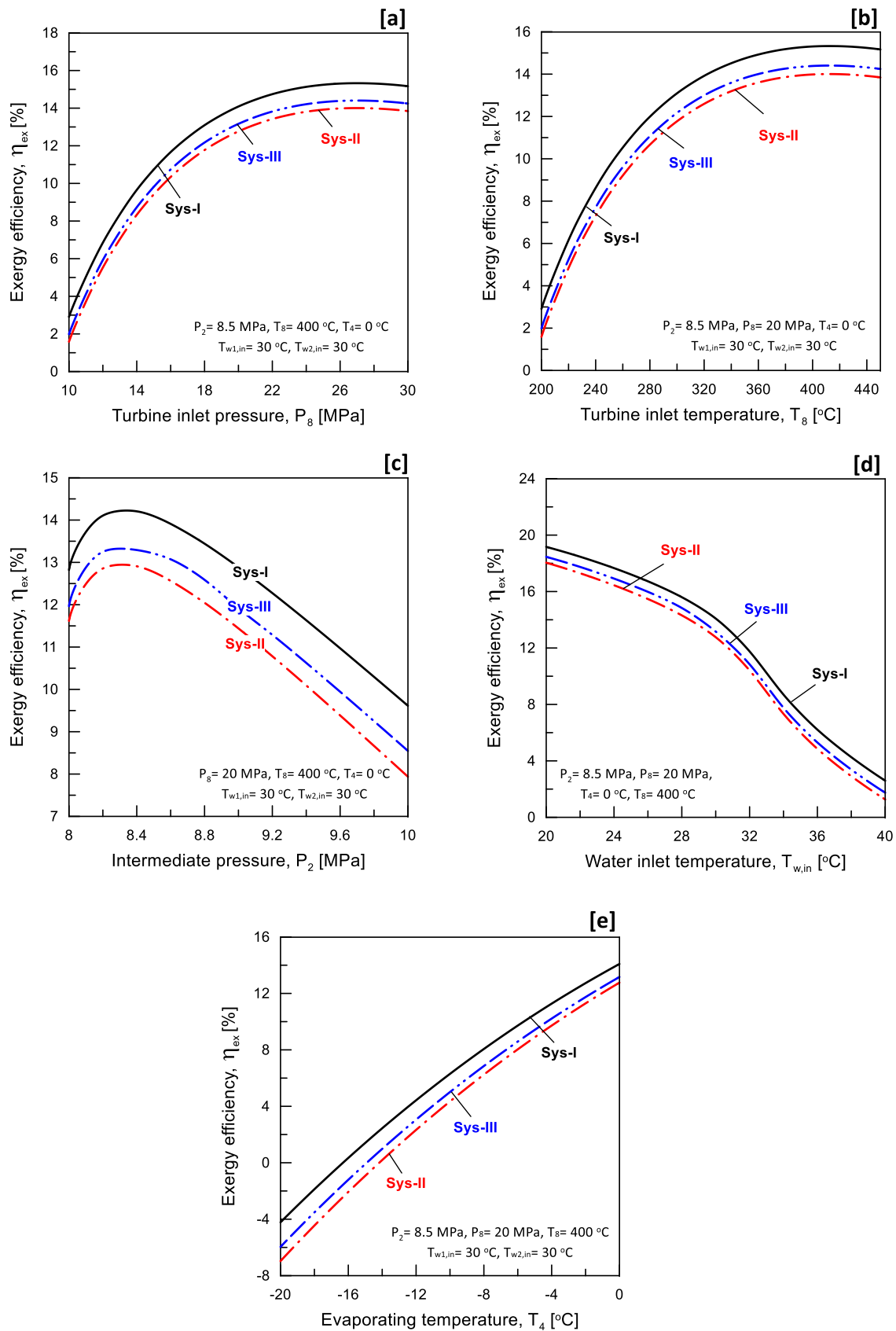
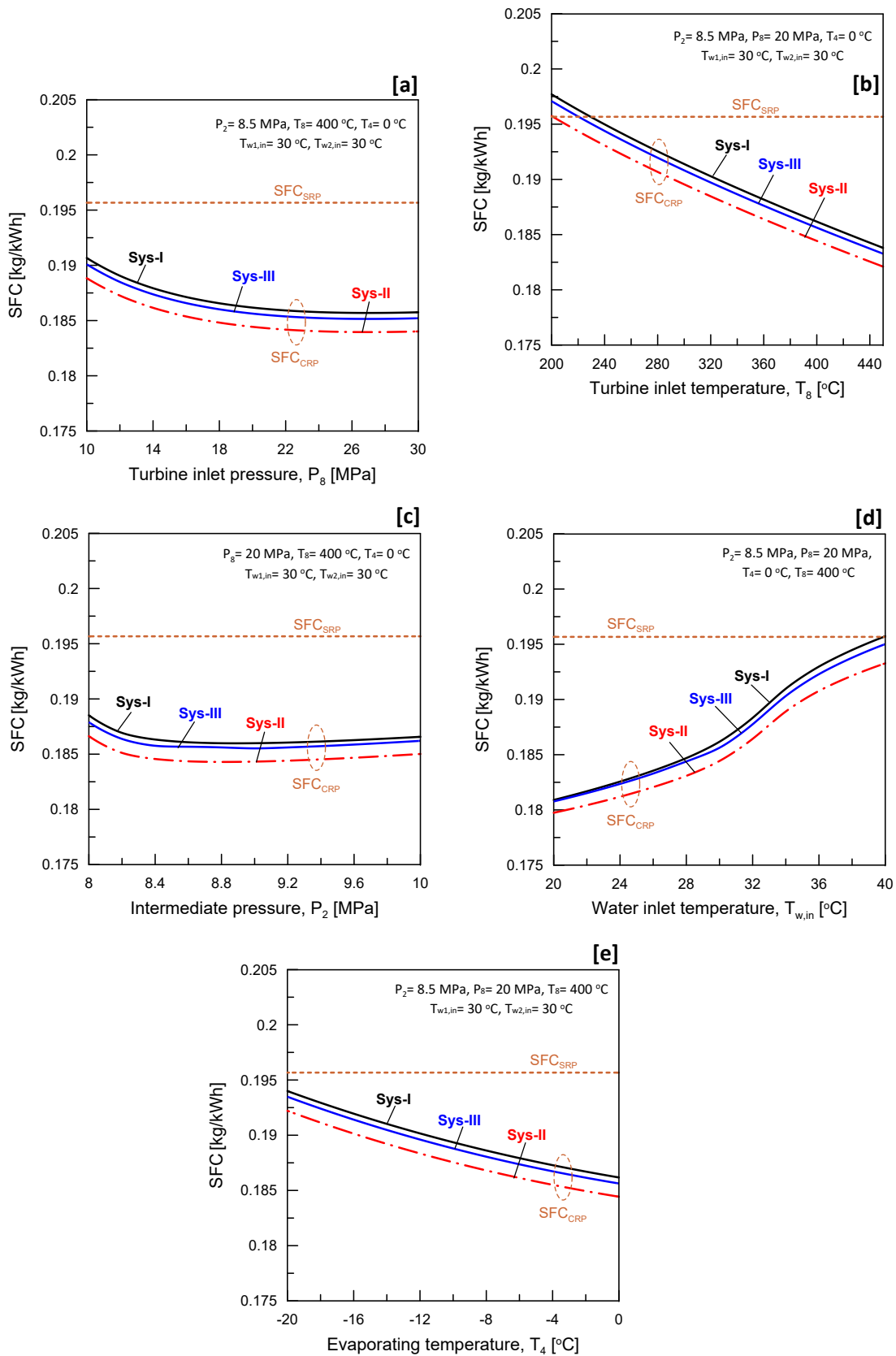


Fig. 7. Variations of exergy efficiency,  $\eta_{ex}$  with various: (a) Turbine inlet pressure; (b) Turbine inlet temperature; (c) Intermediate pressure; (d) Water inlet temperature; (e) Evaporating temperature.



**Fig. 8.** Variations of fuel specific consumption, SFC with various: (a) Turbine inlet pressure; (b) Turbine inlet temperature; (c) Intermediate pressure; (d) Water inlet temperature; (e) Evaporating temperature.

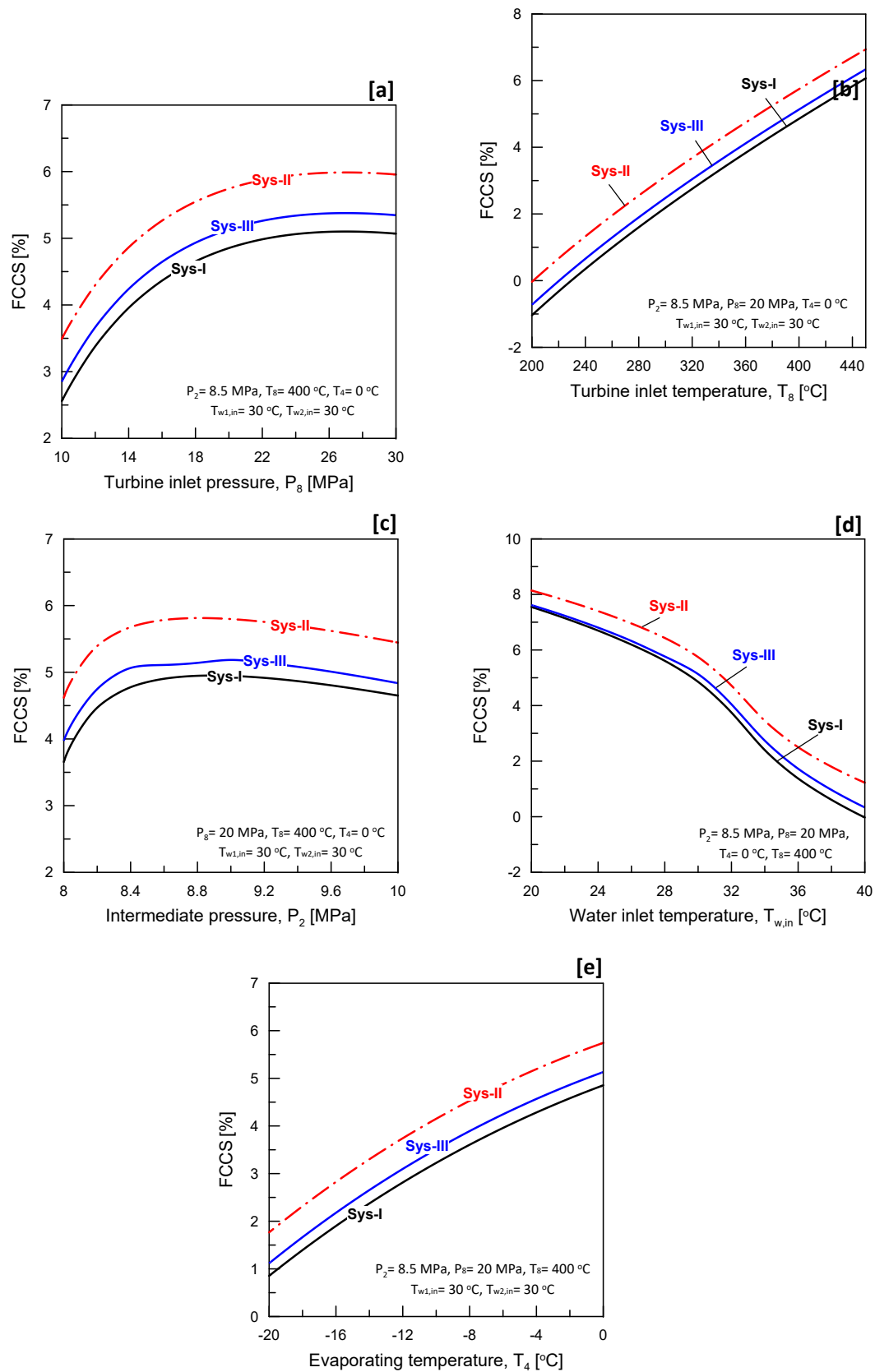


Fig. 9. Variations of fuel consumption cost saving, FCCS with various: (a) Turbine inlet pressure; (b) Turbine inlet temperature; (c) Intermediate pressure; (d) Water inlet temperature; (d) Evaporating temperature.

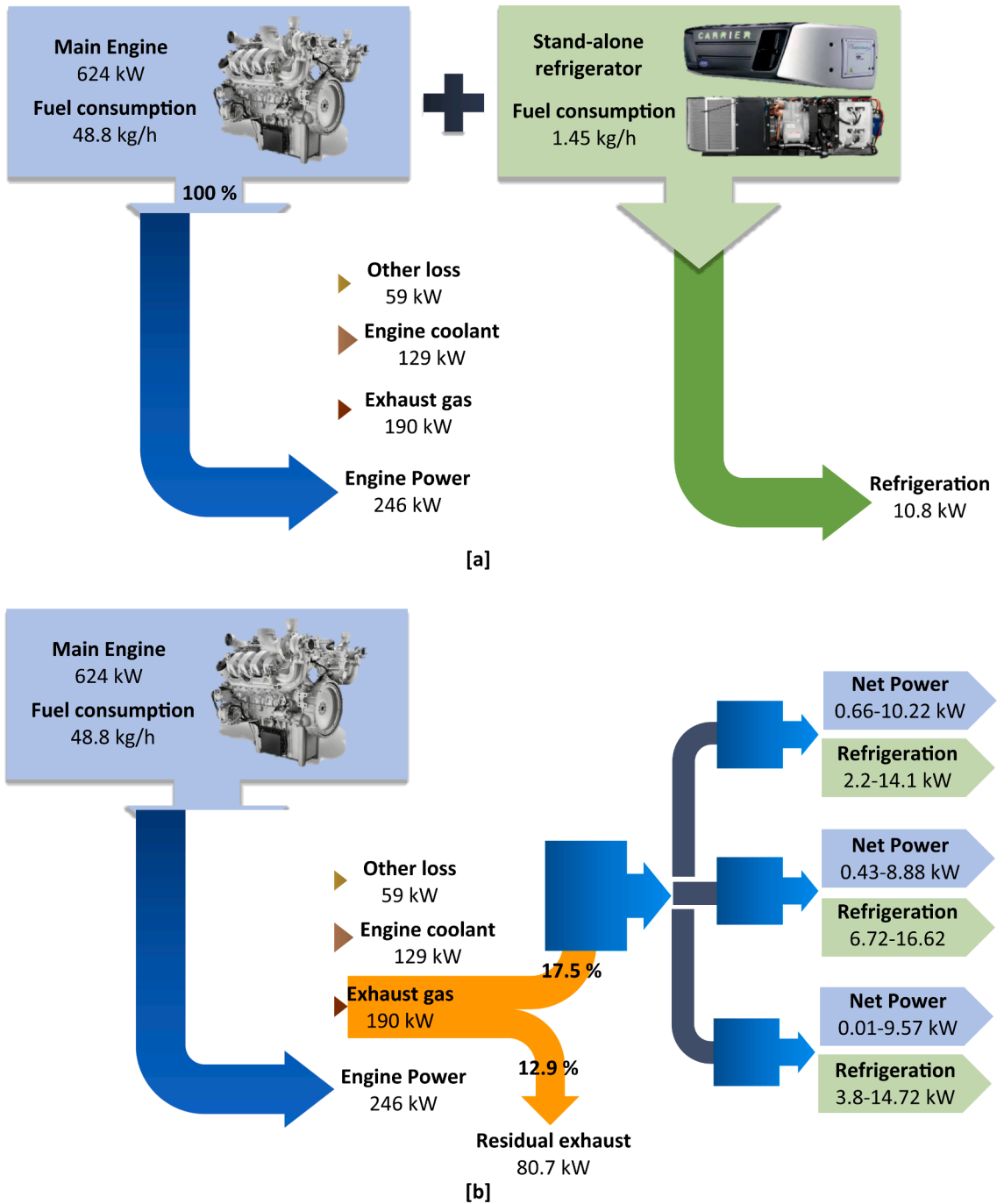


Fig. 10. Energy flow diagram: (a) traditional approach (engine + stand-alone refrigerator); (b) proposed CRP systems (engine + CRP systems).

expressed as follows:

$$\dot{m}_{f,c} = \dot{m}_{f,e} + \dot{m}_{f,t} \quad (1)$$

For the three proposed CRP systems, the energy balance between the turbine and compressors is expressed as follows:

$$\dot{W}_t = (\dot{W}_{Lcomp} + \dot{W}_{Hcomp})/\eta_{t-c} + \dot{W}_{net}/\eta_{gen} \quad (2)$$

For (Sys-I & Sys-II).

$$\dot{m}_{f,t}(h_8 - h_9) = [\dot{m}_{f,c}(h_2 - h_1) + \dot{m}_{f,t}(h_6 - h_{3,1})]/\eta_{t-c} + \dot{W}_{net}/\eta_{gen} \quad (3)$$

For (Sys-III).

$$\dot{m}_{f,t}(h_8 - h_9) = [\dot{m}_{f,c}(h_2 - h_{1,1}) + \dot{m}_{f,t}(h_6 - h_{3,1})]/\eta_{t-c} + \dot{W}_{net}/\eta_{gen} \quad (4)$$

The net power output can be computed as follows:

$$\dot{W}_{net} = (\dot{W}_t - (\dot{W}_{Lcomp} + \dot{W}_{Hcomp})/\eta_{t-c})\eta_{gen} \quad (5)$$

The proposed CRP systems' energy efficiency is defined as follows:

$$\eta_{en} = \frac{\dot{W}_{net} + \dot{Q}_{evap}}{\dot{Q}_{gh}} \quad (6)$$

Table 3 lists the other energy conversion equations for major components and processes.

### 3.2. Exergy analysis

The exergy model is established based on the second law of ther-

**Table 5**  
Optimal parameters for proposed systems based on maximum energy efficiency.

Parameter	Unit	Sys-I	Sys-II	Sys-III
P <sub>1</sub> , P <sub>4</sub> , P <sub>5</sub> , P <sub>9</sub> , P <sub>10</sub> , P <sub>11</sub> ,	Mpa	3.525	3.525	3.525
P <sub>2</sub> , P <sub>3</sub>	Mpa	8.927	9.00	9.00
P <sub>6</sub> , P <sub>7</sub> , P <sub>8</sub>	Mpa	20.76	20.41	20.63
T <sub>1</sub>	°C	26.45	33.92	26.43
T <sub>1,1</sub>	°C	n/a	n/a	29.76
T <sub>2</sub>	°C	113.30	123.20	118.50
T <sub>3</sub> , T <sub>3,1</sub> , T <sub>3,2</sub>	°C	35.00	35.00	35.00
T <sub>3,3</sub>	°C	n/a	26.49	31.54
T <sub>4</sub> , T <sub>5</sub>	°C	0.00	0.00	0.00
T <sub>5,1</sub>	°C	n/a	30.20	n/a
T <sub>6</sub>	°C	65.57	64.17	64.60
T <sub>7</sub>	°C	174.56	173.96	174.35
T <sub>8</sub>	°C	450.00	450.00	450.00
T <sub>9</sub>	°C	301.49	302.84	301.77
T <sub>10</sub>	°C	103.77	100.68	101.86
T <sub>11</sub>	°C	35.00	35.00	35.00
T <sub>EG,in</sub>	°C	470.70	470.70	470.70
T <sub>EG,out</sub>	°C	220.40	220.40	220.40
T <sub>w1,in</sub>	°C	30.00	30.00	30.00
T <sub>w1,out</sub>	°C	43.67	44.57	44.17
T <sub>w2,in</sub>	°C	30.00	30.00	30.00
T <sub>w2,out</sub>	°C	41.10	40.92	40.81
$\dot{m}_{w1}$	Kg/s	1.50	1.50	1.50
$\dot{m}_{w2}$	Kg/s	0.50	0.50	0.50
$\dot{m}_{je}$	g/s	89.00	89.00	89.00
$\dot{m}_{jt}$	g/s	311.00	311.00	311.00
$\dot{W}_{Hcomp}$	kW	7.16	6.87	6.99
$\dot{W}_{Lcomp}$	kW	22.94	24.34	23.81
$\dot{W}_{turbine}$	kW	44.39	44.05	44.32
$\dot{W}_{net}$	kW	9.85	8.44	9.09
$\dot{Q}_{evap}$	kW	10.19	13.84	11.92
$\dot{Q}_{EG}$	kW	109.30	109.30	109.30
$\dot{Q}_{cooler1}$	kW	82.80	88.27	85.87
$\dot{Q}_{cooler2}$	kW	22.42	22.05	21.84
$\dot{Q}_{Reg}$	kW	65.40	66.22	66.05
$\eta_{en}$	%	18.33	20.38	19.22
$\eta_{ex}$	%	19.37	17.36	18.25
SFC	g/kWh	183.40	181.90	182.70
FCCS	%	6.30	7.10	6.60

modynamics to analyze the irreversibility of each component of the proposed CRP systems. The exergy destruction equations of each component of the systems are listed in Table 3. At any state “i” the exergy value is defined as follows:

$$\dot{E}_i = \dot{m}_i [h_i - h_0 - (T_0 + 273.15)(s_i - s_0)] \quad (7)$$

where the subscript ‘0’ denotes the ambient temperature. In this study, the ambient temperature is varied, and the ambient pressure is set to 101.3 kPa. The equations in Table 3 are used to calculate the exergy destruction of the systems’ components.

The refrigeration output exergy is calculated as follows:

$$\dot{E}_{evap} = \dot{Q}_{evap} \left[ \frac{(T_0 + 273.15)}{(T_{ref} + 273.15)} - 1 \right] \quad (8)$$

where T<sub>ref</sub> denotes the temperature of the target cooling environment, which in this study is 2 °C higher than the evaporation temperature (T<sub>evap</sub>).

The systems’ input exergy is defined as follows:

$$\dot{E}_{in} = \dot{E}_{EG,in} - \dot{E}_{EG,out} \quad (9)$$

The proposed CRP systems’ exergy efficiency is defined as follows:

$$\eta_{ex} = \frac{\dot{W}_{net} + \dot{E}_{evap}}{\dot{E}_{in}} \quad (10)$$

### 3.3. Economic analysis

The specific fuel consumption of a given system is defined as follows:

$$SFC \text{ (kg/kWh)} = \frac{\dot{m}_{fuel,total}}{\dot{W}_{Engine} + \dot{W}_{net} + \dot{Q}_{evap}} \quad (11)$$

The specific fuel consumption of the separated engine with stand-alone refrigerator and proposed CRP systems is calculated as follows:

$$SFC_{SRP} \text{ (kg/kWh)} = \frac{\dot{m}_{fuel,engine} + \dot{m}_{fuel,SR}}{\dot{W}_{engine} + \dot{Q}_{evap}} \quad (12)$$

$$SFC_{CRP} \text{ (kg/kWh)} = \frac{\dot{m}_{fuel,engine}}{\dot{W}_{engine} + \dot{W}_{net} + \dot{Q}_{evap}} \quad (13)$$

Table 1 shows the fuel consumption and power of the main engine, as well as the refrigeration capacity of a stand-alone refrigerator.

The percentage of the fuel consumption cost saving (FCCS) parameter is introduced and defined for system evaluation as follows:

$$FCCS \text{ (%) } = \frac{SFC_{SRP} C_{fuel} - SFC_{CRP} C_{fuel}}{SFC_{SRP} C_{fuel}} \times 100 \quad (14)$$

where C<sub>fuel</sub> is fuel unit cost (\$/kg), average world price of diesel is 1.17 \$/L (1.42 \$/kg) [57].

The overview of system modeling is summarized in Table 3. The equations are written in terms of actual state points and can be tailored to the specific components of the proposed CRP system. The modeling assumptions corresponding to realistic component efficiencies, performances, and pressure losses are also summarized.

### 3.4. Model validation

Model validation is used to validate the accuracy of CRP system simulation models created with Aspen HYSYS. Due to the lack of published experiments on the proposed CRP cycle, which consists of a supercritical CO<sub>2</sub> power cycle and a transcritical CO<sub>2</sub> refrigeration cycle, the established S- CO<sub>2</sub> power cycle, or the T- CO<sub>2</sub> refrigeration cycle must be validated independently. The transcritical CO<sub>2</sub> refrigeration cycle with regenerator model has been validated using the same boundary and operating conditions of Rigola et al. [56]. Table 4 compares the current model results to the experimental and numerical results of Rigola et al. [56]. As shown in Table 4, the maximum relative error between the current model’s results and the experimental and numerical results of Rigola et al. [56] is 10.39% for W<sub>comp</sub> and 10.69% for COP, respectively. Which demonstrates that the simulation model approach used in this study via Aspen HYSYS software is sufficiently accurate.

## 4. Results and discussions

The mathematical and simulation model was run using Aspen HYSYS software for comprehensive variations of the operating and controlling parameters including turbine inlet pressure and temperature, intermediate turbine pressure, water inlet temperature, and the evaporator temperature. Each of these parameters was varied in the studied range given in Table 2. In each run processing, the target was calculating the performance parameter of each system (System I, II, and III) including the net power output, refrigeration capacity, energy and exergy efficiencies, specific fuel consumption, and the fuel consumptions cost saving. The obtained comprehensive results data are used to conduct (i) parametric study for the effects of the different operating conditions on the performance parameters of systems I, II, and III, (ii) comparison study to evaluate and compare the three systems at the different operating and controlling conditions (iii) optimization study of the three systems searching for the operating condition that give optimal performance parameters of the three systems. In the following sections the



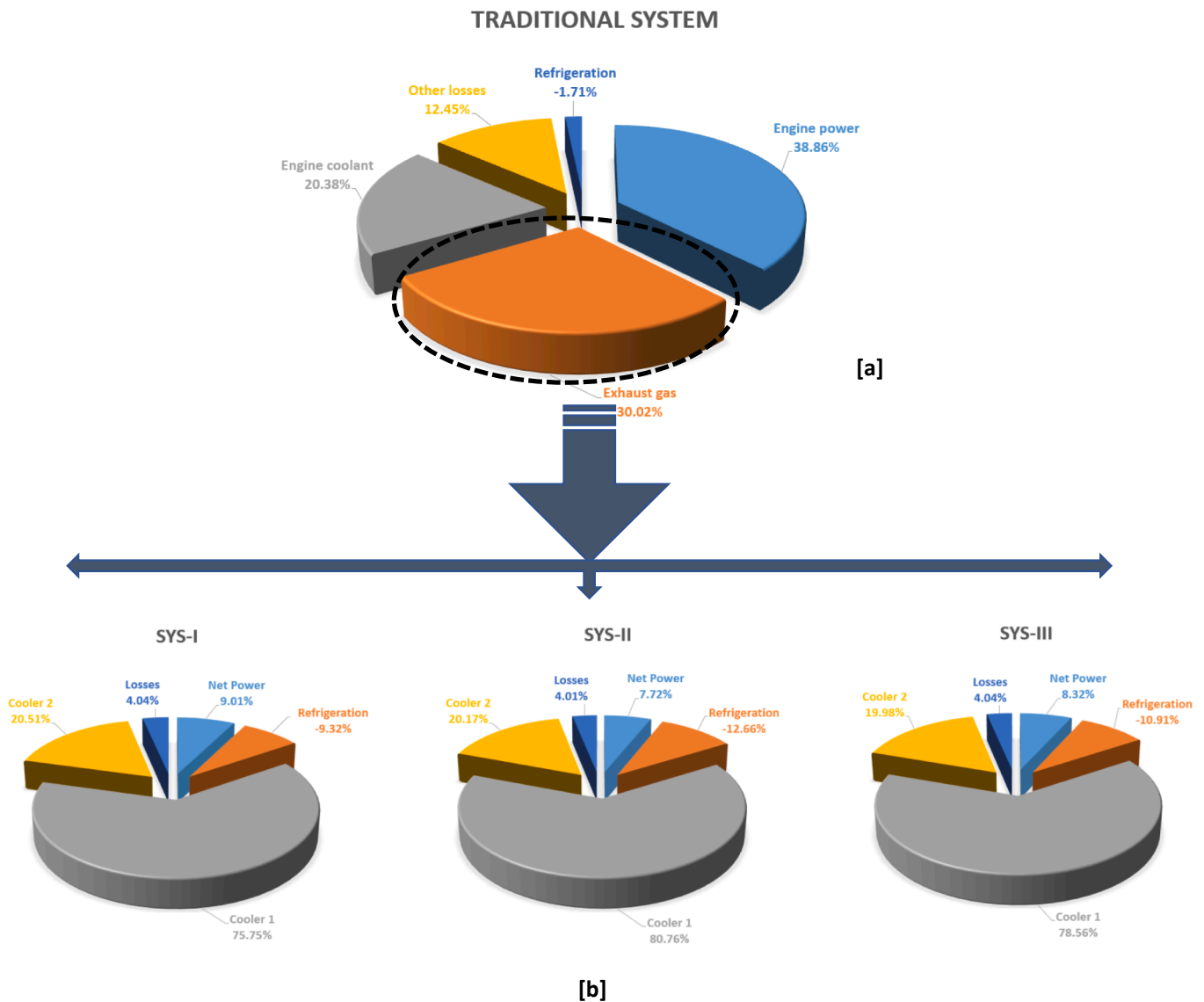


Fig. 11. Output energy breakdown: (a) traditional approach (engine + stand-alone refrigerator); (b) proposed CRP systems (engine + CRP systems).

parametric, comparison and optimization studies of the three proposed systems are discussed in detail.

4.1. Parametric studies of different systems' configurations.

The parametric of the three proposed systems were conducted through investigating the effects of the different operating conditions on the systems performance parameters. The software is used to run and solve the system equations for all the possible combinations of the operating conditions ranges that are given in Table 2. According to the limitation of the paper size, not all the obtained results are presented but only some results are considered and presented. To present the parametric study in an efficient way a base line case of the operating conditions (turbine inlet pressure = 20 MPa, turbine intermediate pressure = 8.5 MPa, turbine inlet temperature = 400 °C, cooling water temperature = 30 °C, evaporator temperature = 0 °C) is considered. To study the effect of a certain parameter of the operating conditions on the systems performances, this parameter will be changed in its entire range (Table 2) and the other parameters of the operating conditions are kept constants at the base line values. Following this technique, the effects of the different operating conditions can be detailed studied as given in the following sections.

4.1.1. Effects of operating conditions on systems' net power outputs

Fig. 4 shows the effect of the turbine inlet pressure and temperature, intermediate turbine pressure, water inlet temperature, and the evaporator temperature on the net power output of the proposed systems I, II, and III. The net power outputs of the three systems are superimposed on the same figures for the sake of the comparisons between the three systems. Fig. 4-a shows the increase of the net power outputs of the three systems with increasing the turbine inlet pressure until 26 bar, then it slightly decreases for any further increasing of the turbine inlet pressure. The trend of variation is the same for the three systems and can be attributed to (i) the increase of the turbine output power due to the increase of the CO<sub>2</sub> enthalpy with increasing its pressure, (ii) the low pressure compressor does not affect with the increase of the pressure at the turbine inlet but the power of the high pressure compressor increases with increasing the turbine inlet pressure, (iii) below 26 bar, the increase in turbine output power with the pressure is higher than the increase of the power of the high pressure compressor and the opposite is true if the turbine inlet pressure is above 26 bar. This trend of variation agrees with the known concept of CO<sub>2</sub> cycles that for power cycle, the turbine inlet pressure need to be high as possible to deliver large power output [58] and for a CO<sub>2</sub> refrigeration cycle [59], the high side pressure (in the present study it is H-compressor pressure which equals to the

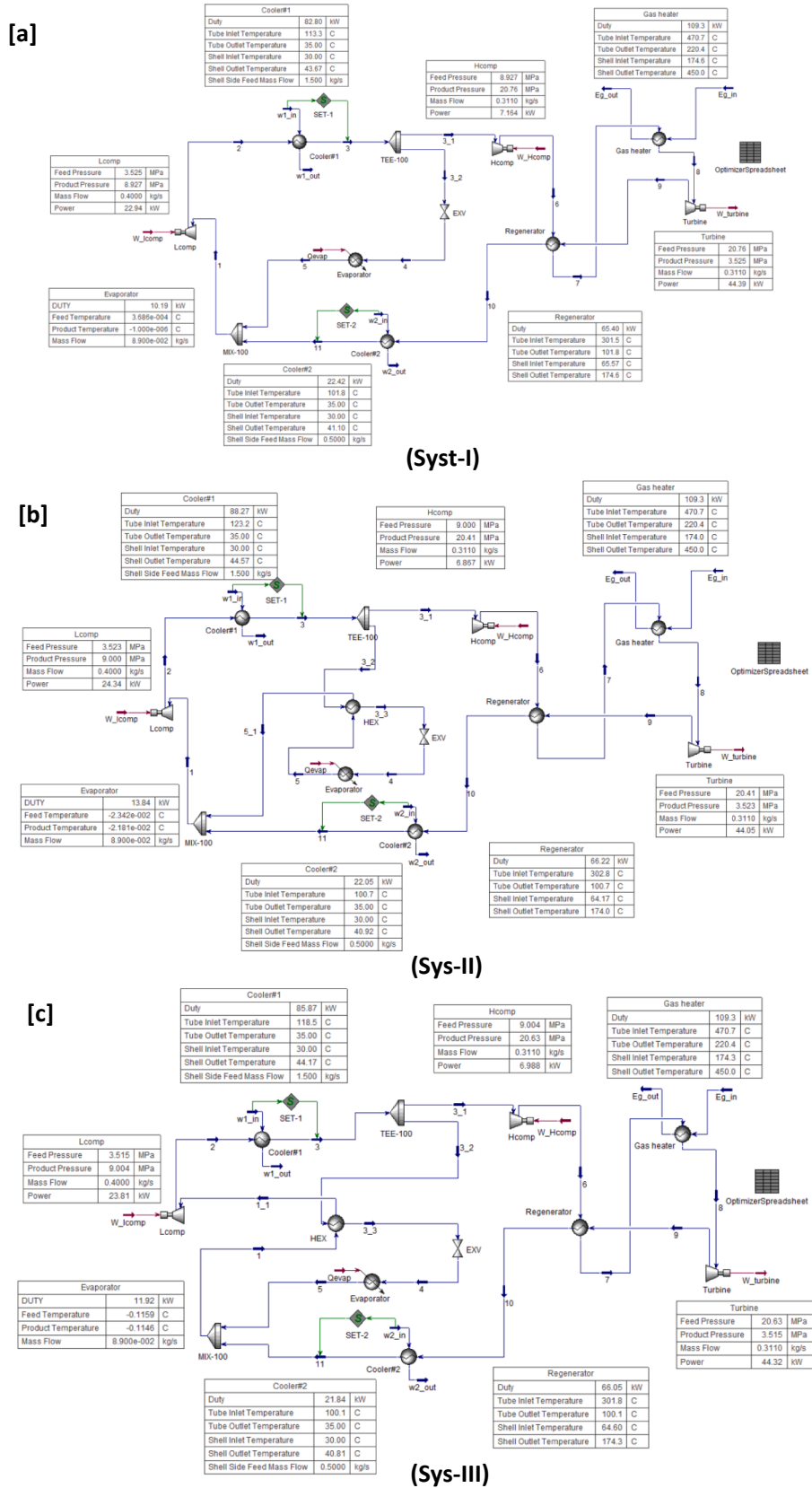


Fig. 12. Systems optimization operating conditions: (a) Sys-I; (b) Sys-II; (c) Sys-III.

**Table 6**

Exergy destruction values and performance for each component based on optimal cases.

Term	Unit	Sys-I	Sys-II	Sys-III
$\dot{I}_{Lcomp}$	kW	3.58	3.71	3.67
$\dot{I}_{Hcomp}$	kW	1.26	1.22	1.24
$\dot{I}_{cooler1}$	kW	5.37	6.34	5.90
$\dot{I}_{cooler2}$	kW	2.00	1.94	1.91
$\dot{I}_{3-way valve}$	kW	0.00	0.00	0.00
$\dot{I}_{EXV}$	kW	1.34	0.95	1.15
$\dot{I}_{evap}$	kW	0.08	0.11	0.10
$\dot{I}_{gh}$	kW	3.79	3.82	3.80
$\dot{I}_{turbine}$	kW	10.39	10.28	10.37
$\dot{I}_{Reg}$	kW	8.94	9.22	9.05
$\dot{I}_{HEX}$	kW	N/A	0.20	0.03
$\dot{I}_{mixer}$	kW	0.19	0.00	0.20
$\dot{E}_{in}$	kW	56.00	56.00	56.00
$\eta_{ex}$	%	19.37	17.36	18.25

turbine inlet pressure) should be as low as possible to reduce the compressor power and provide high coefficient of performance of the refrigeration cycle [58]. This trend is attributed to the shape of the dependent of the compressibility factor of the CO<sub>2</sub> on the pressure.

Fig. 4-b shows the variation of the net output power with the CO<sub>2</sub> gas temperature at the turbine inlet for the three systems. As shown in the figure the net output power of the three systems increases with increasing the turbine inlet temperature and this can be attributed to the direct increase of the enthalpy of the CO<sub>2</sub> gas with increasing its temperature which reflects on the increase of the turbine output power and the net output power of the system. The maximum value of the CO<sub>2</sub> gas temperature at the turbine inlet should not exceeds the exhaust gas temperature (440.7 °C) as the CO<sub>2</sub> gas is heated by the exhaust gas in the regenerator.

Fig. 4-c illustrates the increase of the net output power of the system with increasing the intermediate pressure until it reaches 8.25 bar and then it decreases with any further increase of the intermediate pressure. This can be attributed to the increase of the power of the low-pressure compressor and the decrease of the power of the high-pressure compressor with the increase of the intermediate pressure. Taking in account that the share of the low-pressure compressor in the total compressor power is high compared to the share of the high-pressure compressor as it accommodates the total mass of the CO<sub>2</sub> in the cycle. This trend of the low- and high-pressure compressors power leads to the decrease of the compressor power with the increase of the intermediate pressure until it reaches to 8.25 bar and then the total compressor power increases with increasing the intermediate pressure. This reflects to an opposite trend of the net power output of the system as the turbine outlet power does not affect by the intermediate pressure. This parabolic trend of the compressor power agrees with the variation of the compressibility factor of the CO<sub>2</sub> gas which decrease sharply in the range 8–8.5 MPa and stay with a small value in the range 8.5 MPa–9 MPa [58]. Accordingly, the specific work of the high compressor decreases sharply in the range 8–8.5 MPa and the specific work of the low-pressure compressor linearly increase with increasing the intermediate pressure. This conclude that it is necessary to operate the each of the three systems (I, II, III) at its optimal intermediate pressure that are given in Fig. 4-c to assure maximum net output power of the system.

Fig. 4-d shows the decrease of the net power output of the three systems with the increase of the cooling water temperature (i.e., the increase of the ambient temperature) although the cooling water temperature does not affect the turbine output power. This can be attributed to the increase of the temperature of the CO<sub>2</sub> at the inlets of the low- and high-pressure compressors which leads to the increase of the compressors power and consequently the decrease of the net power output of the system. It was noticed from the results data that the increase in the high

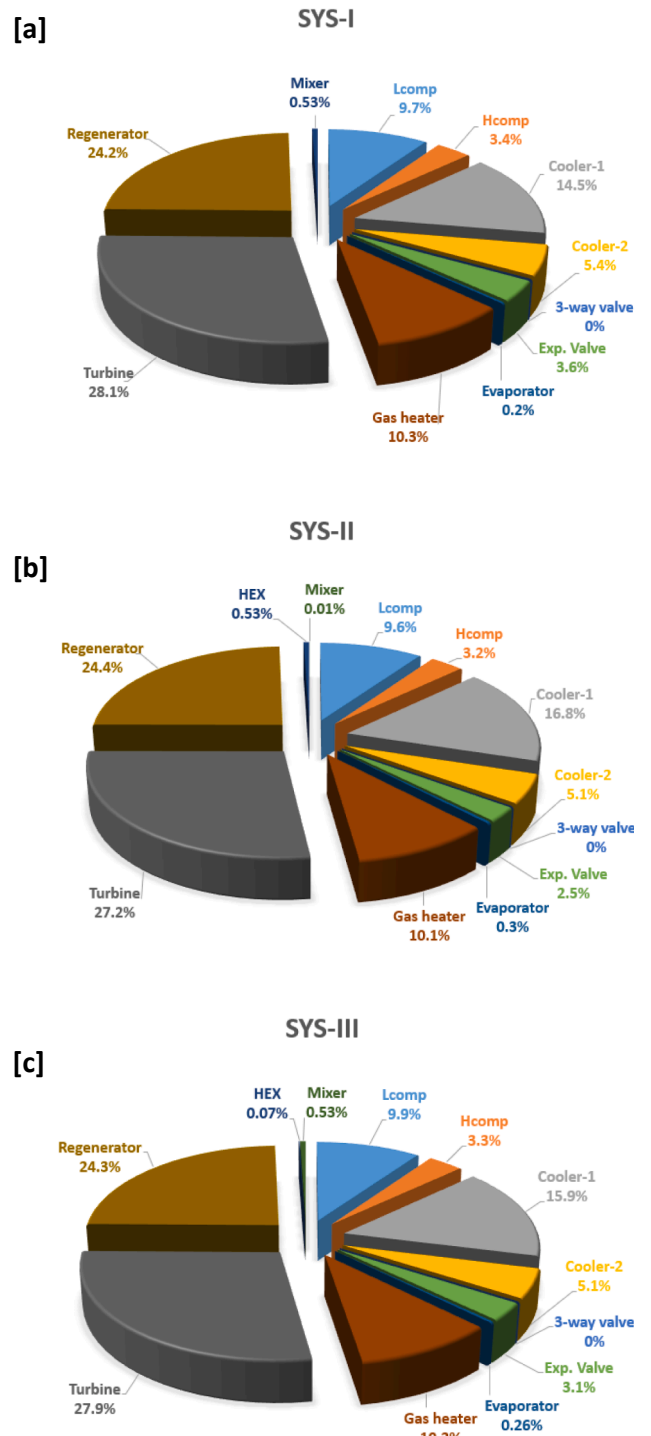


**Fig. 13.** Exergy destruction percentages of each component for optimal cases: (a) Sys-I; (b) Sys-II; (c) Sys-III.

compressor power with the cooling water temperature is higher than that of the low compressor owing to the high compressor is working very close to the area of the large change of CO<sub>2</sub> compressibility which strongly affected by the temperature. Fig. 4-e shows the increase of the net power output of the three systems with the increase of the evaporator temperature, and this can be investigated with detailed inspection of Fig. 2 which shows the decrease of the power of the low-pressure compressor and consequently the increase of the net output power with the increase of the evaporator temperature.

#### 4.1.2. Effects of operating conditions on systems' refrigeration capacities

Fig. 5 shows the effects of the turbine inlet pressure and temperature, intermediate turbine pressure, water inlet temperature, and the evaporator temperature on the refrigeration capacity of the three studied systems I, II, and III. The refrigeration capacities of the three systems are superimposed on the same figures for the sake of the comparisons between the three systems. Fig. 5-a and 5-b show the independence of the refrigeration capacities of the three systems on the turbine inlet pressure and temperature for the entire studied ranges of the other operating parameters. This can be attributed to the independence of the low cycle on the turbine inlet pressure and temperature as both only affect the power high cycle of the system as shown in Fig. 2.

Fig. 5-c illustrates the increase of the refrigeration capacity of the three systems with increasing the intermediate pressure. This can be attributed to that increasing the intermediate pressure causes the states points 3 and 4 of the T-S diagrams given in Fig. 2 moves to the left to be closer to the vertical axes and this cause the increase of the refrigeration effect (h5-h4) which directly reflects on the increase of the refrigeration capacity of the system. Fig. 5-d shows the decrease of the refrigeration capacity of the three systems with the increase of the cooling water temperature. This can be attributed to the increase of the temperature of the CO<sub>2</sub> at the inlets of the expansion valve (State 3) which leads to the movement of State 4 to the right to have higher enthalpy and accordingly the decrease of the refrigeration effect (h5-h4) and the decrease of the refrigeration capacity. Fig. 5-e show the decrease of the refrigeration capacity with the increase of the evaporator temperature. This can be attributed to the shape of the saturation line on the T-S diagram shown in Fig. 2. Increasing the evaporator temperature means the movement of state 5 (Fig. 2) to the left which leads to smaller refrigeration effect and accordingly low refrigeration capacity.

#### 4.1.3. Effects of operating conditions on systems' energy and exergy efficiencies

Figs. 6 and 7 show the effect of the turbine inlet pressure and temperature, intermediate turbine pressure, water inlet temperature, and the evaporator temperature on the energy and exergy efficiencies of the proposed systems I, II, and III. As the energy and exergy efficiencies of the systems directly depend on the net power output and the refrigeration capacity of the system (Eq. 6–9), the variation of the net power output and the refrigeration capacity with the operating conditions that are discussed in sections 4.1.1 and 4.1.2 reflects the trends of the variation of the operating parameters on the energy and exergy efficiencies of the system. Accordingly, Fig. 6 and 7 show the increase of the energy and exergy efficiencies of the system with (i) increasing the turbine inlet temperature and the evaporator temperature, (ii) decreasing the cooling water temperature, (iii) increasing the turbine inlet pressure until reaches to 26 bar and decreasing the turbine inlet pressure above 26 bar, and (iv) increasing the intermediate pressure until 8.2 bar and decreasing the intermediate pressure above 8.2 bar. This can be attributed to the increase of the turbine output power, the decrease of the compressor power and the increase of the refrigeration capacity of the system (refer to Eqs. 6–9) with these parameters in the mentioned ranges.

#### 4.1.4. Effects of operating conditions on systems' specific fuel consumption and cost saving

Fig. 8 shows the effect of the turbine inlet pressure and temperature, intermediate turbine pressure, water inlet temperature, and the evaporator temperature on the specific fuel consumptions of the proposed systems I, II, and III. As shown in the figure the specific fuel consumptions of the three systems decreases with increasing the turbine inlet pressure and temperature, intermediate pressure and the evaporator temperature and increases with increasing the cooling water temperature. This can be attributed to the increase of the sum of the net output work and the refrigeration capacity which reflects directly on the decrease of the specific fuel consumption as given by Eq. (13). Fig. 9

shows the increase of the fuel consumptions cost saving (FCCS) with (i) increasing the turbine inlet temperature and the evaporator temperature, (ii) decreasing the cooling water temperature, (iii) increasing the turbine inlet pressure until reaches to 26 bar and decreasing the turbine inlet pressure above 26 bar, and (iv) increasing the intermediate pressure in the range 0–8.2 bar and decreasing the intermediate pressure in the range >8.2 bar. This can be attributed to the increase of the turbine output power, the decrease of the compressor power and the increase of the refrigeration capacity of the system (refer to Eqs. 6–15) with these parameters in the mentioned ranges.

#### 4.2. Comparisons studies of different systems' configurations

Figs. 4-9 compare the different performance parameters of the three systems in the entire ranges of the operating parameters by superimposing the plotting of the performance curves of the three systems on the same graph. Figs. 4-9 shows that (i) system I has the highest net output power, exergy efficiency and specific fuel consumptions and the lowest refrigeration capacity, energy efficiency and fuel consumption cost saving, (ii) system II has the highest refrigeration capacity, energy efficiency and fuel consumption cost saving and the lowest net output power, exergy efficiency and specific fuel consumption, and (iii) the performance parameters of system III always lies between the values of the performance parameters of system I and II. As discussed before, this can be attributed to that (i) system I has the minimum high compressor power and system II has the maximum high compressor power and system III is between, and (ii) system II has the highest refrigeration capacity and system I has the lowest refrigeration capacity and system III is between.

Fig. 10 gives the energy flow diagrams of the traditional approach (engine + stand-alone refrigerator) and the three proposed CRP systems I, II, and III (engine + CRP systems to drive refrigerator and generate extra power). Fig. 10-a shows that to produce a 246.0 kW engine power and 10.8 kW refrigeration capacity from the traditional engine and the stand-alone refrigeration, the traditional engine consumes 50.25 kg/h fuel (48.8 kg/h for the engine and 1.45 kg/h for the refrigerator). Fig. 10-b shows that including the CRP systems to replace the stand-alone refrigerator and utilizing only 57.5 % of the exhaust gases, the proposed CRP systems saves the fuel consumption of the stand-alone refrigerator and can maintain the needed refrigeration capacity (10.8 kW) or more through the low-pressure cycle, and at the same time can generate an extra power up to 10.22 kW. Therefore, by utilizing 57.7% of the exhaust gases, the CRP systems can achieve a 2.9 % fuel saving (fuel of the refrigerator) and produce 4.4% extra power. Also, the energy flow diagrams shown in Fig. 10 gives the ranges of the net output energy and refrigeration capacity delivered during operating the CRP systems at the entire ranges of the studied operating conditions that are given in Table 2. Fig. 10 shows that the maximum extra net power output (10.26 kW) obtained by CRP systems is given by system I and the maximum refrigeration capacity (16.62 kW) is given by system II.

#### 4.3. System optimization

Optimization study for the three systems is needed to find the operating condition at which the system performance is optimum. The energy efficiency and the specific fuel consumptions can prove and compare the feasibility of the CRP systems and the fuel saving potential. Accordingly, the optimization was conducted based on the energy efficiency as the objective functions, i.e., the optimum operating conditions of each system are the combination of the system operating condition that gives the maximum energy efficiency of the system. To find the optimum operating conditions of each system, the program software is used to solve the system of equations for each system (I, II, III) for all the possible combinations of the operating conditions ranges that are given in Table 2. Then the software is used to search the obtained results to find the operating conditions that give maximum energy efficiency of

the system. Following this technique, Table 5 lists the optimal operating conditions and the values of the optimum performance parameters for each system. Also, Fig. 11 gives the operating conditions and input/output energy of each component of each system at the optimal operating conditions of the system. Table 5 shows that the optimum performance parameters (energy efficiency, specific fuel consumptions and fuel consumption cost savings) of systems I, II, III are (18.3%, 0.1834 kg/kWh, 6.3%), (20.4%, 0.1819 kg/kWh, 7.1%), and (19.3%, 0.1827 kg/kWh, 6.36%), respectively. The operating conditions (turbine inlet pressure, turbine intermediate pressure, cooling water temperature, evaporator temperature) that give these optimum performance parameters of the three systems I, II, III are (20.76 MPa, 450 °C, 8.927 MPa, 30.00 °C and 0.00 °C), (20.41 MPa, 450 °C, 9.00 MPa, 30.00 °C and 0.00 °C), and (20.63 MPa, 450 °C, 9 MPa, 30.00 °C and 0.00 °C), respectively. The optimum turbine inlet temperature, cooling water temperature and evaporator temperature are the same for the three systems because the performance parameters of the three systems are directly proportional to these operating conditions in their entire ranges as shown in Figs. 4-9. Comparing the performance parameters of the three systems, reveals that system II has the absolute optimum performance with values energy efficiency = 20.4%, specific fuel consumptions = 0.1819 kg/kWh and fuel consumption cost savings = 7.1%. and occurs at turbine inlet pressure, turbine intermediate pressure, cooling water temperature, evaporator temperature of 20.41 MPa, 450 °C, 9.00 MPa, 30.00 °C and 0.00 °C, respectively.

Fig. 12 shows the energy balance chart of the traditional system and the CRP three systems at their optimal operating conditions. In this figure, all the amount of the exhaust gases are used to drive the CRP systems. As shown in Fig. 11-b, about 18.33%, 20.38% and 19.22% of the energy of the exhaust gases (which represents 30% of the fuel energy) can be recovered by CRP systems I, II, and III, respectively to convert about 9.01%, 7.72% and 8.32% of the exhaust gas energy to output power and 9.32%, 12.66% and 10.91% of it to drive the refrigeration cycle for system I, II, III, respectively.

Exergy analysis of each component of the three systems as well as for the entire system are conducted to study the irreversibility and the exergy destruction of each component of the three systems. The exergy analysis is carried out at the optimal operating conditions and based on the optimization data. Table 6 and Fig. 13 give the exergy destruction of each component of the three systems and the exergy efficiencies of the three systems at their optimum operating conditions. Table 6 and Fig. 13 show that the components of the systems that have highest values of exergy destructions are the turbine, then the generator and then cooler I and the heat exchanger. Although system II has the optimum energy efficiency among the three system, Table 6 and Fig. 13 shows that system I has the highest value of the exergy efficiency (19.37%) at the optimum operating conditions and system II has the lowest value of the exergy efficiency (17.36) at the optimum operating conditions. This small difference can be attributed to the extra components of system II that are not included in system I like the heat exchanger and due to the different in optimal operating conditions of the two systems.

## 5. Conclusions

The present study proposed and compared the performance of three CRP systems to cover the refrigeration capacity of the traditional approach (engine + stand-alone refrigerator) of a refrigerated truck and produce extra power (engine + CRP systems to drive refrigerator and generate extra power). CO<sub>2</sub> is used as the working fluid for the low and high pressures combined refrigeration and power cycles. The feasibility of the using CRP systems was justified and has proven the potential of energy and fuel consumption saving compared to the traditional engine + stand-alone refrigerator. The proposed modifications on the basic CRP system (System I) by incorporated heat exchanger for energy recovery at two different locations of the cycle (System II and System III) was investigated and has proven its potential for higher energy efficiency of

the system as well as higher refrigeration capacity. Parametric and optimization studies were conducted to show the effect of the different operating parameters on the three proposed systems and find the optimal operating conditions of each system that gives maximum energy efficiency of the system. The main conclusions of the results of the present study can be summarized in the following points are as follows:

1. The proposed CRP system has proven its potential to replace the tradition engine and the stand-alone refrigerator and utilize only 57.7% of the exhaust gases to cover the needed refrigeration capacity and produce 4.8% power increase and 2.9% fuel saving.
2. The proposed CRP systems I, II, III can utilize all the exhaust gases to recover about 18.33%, 20.38% and 19.22% of the energy of the exhaust gases (which represents 30% of the engine fuel energy), and convert about 9.01%, 7.72% and 8.32% of the exhaust gas energy to output power and 9.32%, 12.66% and 10.91% of it to drive the refrigeration cycle for system I, II, III, respectively.
3. The parametric study showed the effects of the different operating conditions (turbine inlet pressure and temperature, intermediate pressure, cooling water and evaporator temperatures) on the performance parameters (net output power, refrigeration capacity, energy and exergy efficiencies, specific fuel consumptions and fuel cost saving) for the three systems.
4. Comparison study of the three systems showed that system I has the highest net output power, exergy efficiency and specific fuel consumptions and system II has the highest refrigeration capacity, energy efficiency and fuel consumption cost saving. The maximum extra net power output (10.26 kW) obtained by using CRP systems is given by system I and the maximum refrigeration capacity (16.62 kW) is given by system II.
5. Optimization reveals the optimum performance parameters (energy efficiency, specific fuel consumptions and fuel consumption cost savings) of systems I, II, III are (18.3%, 0.1834 kg/kWh, 6.3%), (20.4%, 0.1819 kg/kWh, 7.1%), and (19.3%, 0.1827 kg/kWh, 6.36%), respectively.

## CRedit authorship contribution statement

**H.F. Elattar:** Data curation, Methodology. **S.A. Nada:** Conceptualization, Methodology, Writing – review & editing.

## Declaration of Competing Interest

The authors declare that they have no known competing financial interests or personal relationships that could have appeared to influence the work reported in this paper.

## References

- [1] BP Statistical Review of World Energy June 2017. <http://www.bp.com/content/dam/bp/en/corporate/pdf/energy-economics/statistical-review-2017/bp-statistical-review-of-world-energy-2017-full-report.pdf>.
- [2] Attia AMA, Nour M, Nada SA. Study of Egyptian castor biodiesel-diesel fuel properties and diesel engine performance for a wide range of blending ratios and operating conditions for the sake of the optimal blending ratio. *Energy Convers Manage* 2018;174:364–77.
- [3] Attia AMA, Nour M, El-Seesy A, Nada SA. The effect of castor oil methyl ester blending ratio on the environmental and the combustion characteristics of diesel engine under standard testing conditions. *Sustainable Energy Technol Assess* 2020; 42:100843.
- [4] Attia AMA, Kulchitskiy AR, Nour M, El-Seesy A, Nada SA. The influence of castor biodiesel blending ratio on engine performance including the determined diesel particulate matters composition. *Energy* 2022;239:121951.
- [5] Nour M, Nada SA, Li X. Experimental study on the combustion performance of a stationary CIDI engine fueled with 1-heptanol-diesel mixtures. *Fuel* 2022;312: 122902.
- [6] Nour M, El-Seesy A, Attia AMA, Nada SA. Adding n-butanol, n-heptanol, and n-octanol to improve vaporization, combustion, and emission characteristics of diesel/used frying oil biodiesel blends in DICl engine. *Environ Progr Sustainable Energy* 2020;40(3). e13549.

- [7] Nour M, Attia AMA, Nada SA. Improvement of CI engine combustion and performance running on ternary blends of higher alcohol (Pentanol and Octanol)/hydrous ethanol/diesel. *Fuel* 2019;251:10–22.
- [8] Nour M, Attia AMA, Nada SA. Combustion, performance and emission analysis of diesel engine fueled by higher alcohols (butanol, octanol and heptanol)/diesel blends. *Energy Convers Manage* 2019;185:313–29.
- [9] Xia Y, Wang J, Lou J, Zhao P, Dai Y. Thermo-economic analysis and optimization of a combined cooling and power (CCP) system for engine waste heat recovery. *Energy Convers Manage* 2016;128:303–16.
- [10] Shu G, Che J, Hua T, Wang X, Liu P. A compressor-assisted triple-effect H<sub>2</sub>O-LiBr absorption cooling cycle coupled with a Rankine Cycle driven by high-temperature waste heat. *Appl Therm Eng* 2016;112:1626–37.
- [11] Singh OK, Yan J. Performance enhancement of combined cycle power plant using inlet air cooling by exhaust heat operated ammonia-water absorption refrigeration system. *Appl Energy* 2016;180:867–79.
- [12] Lu Y, Wang Y, Dong C, Wang L, Roskilly AP. Design and assessment on a novel integrated system for power and refrigeration using waste heat from diesel engine. *Appl Therm Eng* 2015;91:591–9.
- [13] Liang Y, Shu G, Hua T, Liang X, Wei H, Liu L. Analysis of an electricity-cooling cogeneration system based on RC-ARS combined cycle aboard ship. *Energy Convers Manage* 2013;76(1):1053–60.
- [14] Ifaei H, Ataie A, Yoo CK. Thermoeconomic and environmental analyses of a low water consumption combined steam power plant and refrigeration chillers-Part 2: Thermoeconomic and environmental analysis. *Energy Convers Manage* 2016;123:625–42.
- [15] Wang J, Wang J, Zhao P, Dai Y. Thermodynamic analysis of a new combined cooling and power system using ammonia–water mixture. *Energy Convers Manage* 2016;117:335–42.
- [16] Yu G, Shu G, Tian H, Huo Y, Zhu W. Experimental investigations on a cascaded steam-organic-Rankine-cycle (RC/ORC) system for waste heat recovery (WHR) from diesel engine. *Energy Convers Manage* 2016;129:43–51.
- [17] Neto RDO, Coronado CJR, Nascimento MAR. Technical and economic analyses of waste heat energy recovery from internal combustion engines by the Organic Rankine Cycle. *Energy Convers Manage* 2016;129:168–79.
- [18] Xu B, Rathod D, Yebi A, Filipi Z. Real-time realization of Dynamic Programming using machine learning methods for IC engine waste heat recovery system power optimization. *Appl Energy* 2020;262:114514.
- [19] Shi L, Shu G, Tian H, Huang G, Chen T, Li X, et al. Experimental comparison between four CO<sub>2</sub>-based transcritical Rankine cycle (TRC) systems for engine waste heat recovery. *Energy Convers Manage* 2017;150:159–71.
- [20] Song J, Li X, Ren X, et al. Performance improvement of a preheating supercritical CO<sub>2</sub> (S-CO<sub>2</sub>) cycle based system for engine waste heat recovery. *Energy Convers Manage* 2018;161:225–33.
- [21] Shi L, Shu G, Tian H, Chen T, Liu P, Li L. Dynamic tests of CO<sub>2</sub>-Based waste heat recovery system with preheating process. *Energy* 2019;171:270–83.
- [22] Yoro, K.O.; Daramola, M.O. Chapter 1—CO<sub>2</sub> emission sources, greenhouse gases, and the global warming effect. In *Advances in Carbon Capture*, 1st ed.; Rahimpour, M.R., Farsi, M., Makarem, M.A., Eds.; Woodhead Publishing: Sawston, UK, 2020; pp. 3–28, ISBN 9780128196571.
- [23] Adavi K, Dehkordi AM. Synthesis and polymorph controlling of calcite and aragonite calcium carbonate nanoparticles in a confined impinging-jets reactor. *Chem Eng Process Process Intensif* 2021;159:108239.
- [24] Song J, Li X-S, Ren X-D, Gu C-W. Performance analysis and parametric optimization of supercritical carbon dioxide (S-CO<sub>2</sub>) cycle with bottoming Organic Rankine Cycle (ORC). *Energy* 2018;143:406–16.
- [25] He C, Liu C, Zhou M, Xie H, Xu X, Wu S, et al. A new selection principle of working fluids for subcritical organic Rankine cycle coupling with different heat sources. *Energy* 2014;68:283–91.
- [26] Crespi F, Gavagnin G, Sanchez D, Martínez GS. Supercritical carbon dioxide cycles for power generation: a review. *Appl Energy* 2017;195:152–83.
- [27] D. Di Battista, F. Fatigati, R. Carapellucci, R. Cipollone, An improvement to waste heat recovery in internal combustion engines via combined technologies. *Energy Convers Manage* 232 (2021) 113880, <https://doi.org/10.1016/j.enconman.2021.113880>.
- [28] Llopis R, Nebot-Andrés L, Sánchez D, Catalán-Gil J, Cabello R. Subcooling methods for CO<sub>2</sub> refrigeration cycles: a review. *Int J Refrig* 2018;93:85–107.
- [29] Hou S, Zhang F, Yu L, Cao S, Zhou Y, Wu Y. Optimization of a combined cooling, heating and power system using CO<sub>2</sub> as main working fluid driven by gas turbine waste heat. *Energy Convers Manage* 2018;178:235–49.
- [30] Xu X, Liu C, Fu X, Gao H, Li Y. Energy and exergy analyses of a modified combined cooling, heating, and power system using supercritical CO<sub>2</sub> energy.
- [31] Javier Cardenas Gutierrez, Guillermo Valencia Ochoa, Jorge Duarte-Forero. A comparative study of the energy, exergetic and thermo-economic performance of a novelty combined Brayton S-CO<sub>2</sub>-ORC configurations as bottoming cycles, *Heliyon* 6 (2020) e04459.
- [32] Sun X, Shi L, Tian Ha, Wang X, Zhang Y, Shu G. A novel composition tunable combined cooling and power cycle using CO<sub>2</sub>-based binary zeotropic mixture. *Energy Convers Manage* 2021;244:114419.
- [33] Anjan Kumar Sahu, Neeraj Agrawal, Prasant Nanda, A parametric study of transcritical CO<sub>2</sub> simple cooling cycle and combined power cycle, *Int J Low-Carbon Technol* 2017, 12, 383–391.
- [34] Wang Z, Jiang Y, Han F, Shui Y, Li W, Ji Y, et al. A thermodynamic configuration method of combined supercritical CO<sub>2</sub> power system for marine engine waste heat recovery based on recuperative effects. *Appl Therm Eng* 2022;200:117645.
- [35] Nader WB, Mansour C, Dumand C, Nemer M. Brayton cycles as waste heat recovery systems on series hybrid electric vehicles. *Energy Convers Manage* 2018;168:200–14.
- [36] Song Y, Wang H, Ma Y, Yin X, Cao F. Energetic, economic, environmental investigation of carbon dioxide as the refrigeration alternative in new energy bus/railway vehicles' air conditioning systems. *Appl Energy* 2022;305:117830.
- [37] Song X, Daxiong Lu, Lei Q, Wang D, Binbin Y, Shi J, et al. Energy and exergy analyses of a transcritical CO<sub>2</sub> air conditioning system for an electric bus. *Appl Therm Eng* 2021;190:116819.
- [38] Fartaj A, Ting D-K, Yang WW. Second law analysis of the transcritical CO<sub>2</sub> refrigeration cycle. *Energy Convers Manage* 2004;45:2269–81.
- [39] Sharma OP, Kaushik SC, Manjunath K. Thermodynamic analysis and optimization of a supercritical CO<sub>2</sub> regenerative recompression Brayton cycle coupled with a marine gas turbine for shipboard waste heat recovery. *Thermal Sci Eng Progr* 2017;3:62–74.
- [40] Zhang R, Wen S, Lin X, Zhou N, Zhao L. Thermodynamic analysis and parametric optimization of a novel SeCO<sub>2</sub> power cycle for the waste heat recovery of internal combustion engines. *Energy* 2020;209:118484.
- [41] Ouyang T, Zhang M, Mo X, Qin P. Transient characteristic evaluation and optimization of supercritical CO<sub>2</sub> Brayton cycle driven by waste heat of automotive gasoline engine. *J Cleaner Prod* 2021;329:129796.
- [42] Shi L, Tian Ha, Shu G. Multi-mode analysis of a CO<sub>2</sub>-based combined refrigeration and power cycle for engine waste heat recovery. *Appl Energy* 2020;264:114670.
- [43] Musharavati F, Khanmohammadi S, Pakseresht A, Khanmohammadi S. Comparative analysis and multi-criteria optimization of a supercritical recompression CO<sub>2</sub> Brayton cycle integrated with thermoelectric modules. *J Therm Anal Calorim* 2021;145:769–85.
- [44] Daniel Sánchez, Jorge Patiño, Rodrigo Llopis, Ramón Cabello, Enrique Torrella, Fernando Vicente Fuentes, New positions for an internal heat exchanger in a CO<sub>2</sub> supercritical refrigeration plant. Experimental analysis and energetic evaluation, *Appl Thermal Eng* 63 (2014) 129e139.
- [45] Wang S, Liu C, Li J, Sun Z, Chen X, Wang X. Exergoeconomic analysis of a novel trigeneration system containing supercritical CO<sub>2</sub> Brayton cycle, organic Rankine cycle and absorption refrigeration cycle for gas turbine waste heat recovery. *Energy Convers Manage* 2020;221:113064.
- [46] Gang Li, Magnus Eisele, Hoseong Lee, Yunho Hwang, Reinhard Radermacher, Experimental investigation of energy and exergy performance of secondary loop automotive air-conditioning systems using low-GWP (global warming potential) refrigerants, *Energy* 68 (2014) 819e831.
- [47] Xin T, Cheng Xu, Yang Y. Thermodynamic analysis of a novel supercritical carbon dioxide Brayton cycle based on the thermal cycle splitting analytical method. *Energy Convers Manage* 2020;225:113458.
- [48] Banik S, Ray S, De S. Thermodynamic modelling of a recompression CO<sub>2</sub> power cycle for low temperature waste heat recovery. *Appl Therm Eng* 2016;107:441–52.
- [49] Mohanraj M, Andrew Pon Abraham JD. Environment friendly refrigerant options for automobile air conditioners: a review. *J Thermal Anal Calorim* 2020. <https://doi.org/10.1007/s10973-020-10286-w>.
- [50] Vashisht S, Rakshit D. Recent advances and sustainable solutions in automobile air conditioning systems. *J Cleaner Prod* 2021;329:129754.
- [51] Rony RU, Yang H, Krishnan S, Song J. Recent advances in transcritical CO<sub>2</sub> (R744) heat pump system: a review. *Energies* 2019;12:457. <https://doi.org/10.3390/en12030457>.
- [52] Dilshad S, Kalair AR, Khan N. Review of carbon dioxide (CO<sub>2</sub>) based heating and cooling technologies: past, present, and future outlook. *Int J Energy Res* 2020;44:1408–63.
- [53] Barta RB, Groll EA, Ziviani D. Review of stationary and transport CO<sub>2</sub> refrigeration and air conditioning technologies. *Appl Therm Eng* 2021;185:116422.
- [54] Aspen HYSYS V8.6. [www.aspentech.com](http://www.aspentech.com). 2014.
- [55] Yao Y, Shi L, Tian H, Wang X, Sun X, Zhang Y, Zirui W, Sun R, Shu G. Combined cooling and power cycle for engine waste heat recovery using CO<sub>2</sub>-based mixtures. *Energy* 2022;240:122471.
- [56] Rigola J, Raush G, Pérez-Segarra CD, Oliva A. Numerical simulation and experimental validation of vapour compression refrigeration systems. Special emphasis on CO<sub>2</sub> trans-critical cycles. *Int J Refrig* 2005;28:1225–37.
- [57] Global petrol prices. [https://www.globalpetrolprices.com/diesel\\_prices/](https://www.globalpetrolprices.com/diesel_prices/). February 2022.
- [58] Bellos E, Tzivanidis C. A comparative study of CO<sub>2</sub> refrigeration systems. *Energy Convers Manage* X 2019;1:100002.
- [59] Kim YM, Sohn JL, Yoon ES. Supercritical CO<sub>2</sub> Rankine cycles for waste heat recovery from gas turbine. *Energy* 2017;118:893–905.